Energy exchange between a relativistic polytrope and a Wyman IIa fluid

Journal:	*European Physical Journal C*
Manuscript ID	Draft
Manuscript Type:	Regular Article
Date Submitted by the Author:	n/a
Complete List of Authors:	Andrade Landeta, Julio; Escuela Superior Politécnica de Chimborazo Naseer, Tayyab; The University of Lahore - Raiwind Road Campus, Mathematics and Statistics
Note: The following files were submitted by the author for peer review, but cannot be converted to PDF. You must view these files (e.g. movies) online.	
example.eps	

Eur. Phys. J. C manuscript No.
(will be inserted by the editor)

Energy exchange between a relativistic polytrope and a Wyman IIa fluid

Jorge Gallegos [1], **Doménica Quizhpe**[1], **J. Andrade**[a,1], **Marlon Moscoso-Martínez**[b,1,2], **Tayyab Naseer** [c,3,4]

[1]Escuela Superior Politécnica de Chimborazo, (ESPOCH), Riobamba 060155, Ecuador
[2]Higher School of Engineering and Technology, Universidad Internacional de la Rioja (UNIR), Avda. de la Paz 137, Logroño, 26006, España
[3]Department of Mathematics and Statistics, The University of Lahore, 1-KM Defence Road, Lahore 54000, Pakistan
[4]Research Center of Astrophysics and Cosmology, Khazar University, Baku, AZ1096, 41 Mehseti Street, Azerbaijan

Received: date / Accepted: date

Abstract A detailed analysis of the energy exchange between a relativistic polytrope and an isotropic Wyman IIa fluid within a compact stellar object is presented. This investigation uses the theoretical framework of gravitational decoupling by extended minimal geometric deformation as its central axis. The results show that the polytrope transfers energy to the Wyman IIa fluid in the outer layers of the system, while the core remains stable without any energy transfer. Furthermore, it is verified that the effective compact system is physically realistic for configurations satisfying the well-known strong energy condition for anisotropic self-gravitating spheres, since its violation in this case leads to unstable configurations.

1 Introduction

One of the best natural laboratories for exploring the limits of physical knowledge is stellar remnants. Such astrophysical configurations are notable for their extreme conditions, such as high density, strong magnetic fields, high temperatures, and so on. Specifically, their high density leads to the generation of high gravitational fields, which can even tear the fabric of spacetime apart in the extreme case of black holes. This is why the use of the modern theory of general relativity is essential to unravel their mysteries, given that the use of Newtonian gravitation is no longer reliable in these extreme regimes. The theoretical study of these fascinating objects began with the discovery of the first solution to Einstein's Field Equations (EFE) [1, 2] by K. Schwarzschild, both as an internal and external solution of an isotropic, homogeneous, self-gravitating sphere [3, 4]. Later, solutions in the isotropic pressure regime were found; for example, works such as [5–16]. Such solutions, however, do not fully describe more realistic stellar systems since they present local deviation from isotropy due to various aspects that are very specific to these astrophysical objects, such as their high density, strong magnetic fields, rotation, high temperature, internal phase transitions, presence of solid cores, etc [17–30]. Indeed, this aspect has been demonstrated to be a result of the stellar evolution of these objects [31], and therefore results in a physical interest in the construction of this kind of model in the regimen of anisotropic pressure.

The first hint of the real possibility of the presence of anisotropy in stellar fluids due to stellar velocity dispersion was developed by Jean in [32]. Indeed, Einstein noticed that the spherical symmetry in EFE maintains equality only in the two tangential pressures, and subsequently this was indicated also by Lemaitre in 1933 [33]. This fact has been reinforced by Ruderman, who showed theoretically that in very high-density regimes typical of stellar remnants larger than $10^{15}\ g/cm^3$, the anisotropy in pressures seems to be a natural aspect. Subsequently, Bowers and Liang examined this aspect in [34]. They found that anisotropy plays a very important role in the stability of stellar remnants and that it is more likely to occur in the outer parts of compact stars than in the core. Subsequently, many studies have been carried out – multiple subsequent studies that take into account the anisotropy in the interior of these fascinating astrophysical objects, such as [35–42].

[a]e-mail: julio.andrade@espoch.edu.ec
[b]e-mail: marlon.moscoso@espoch.edu.ec;marlonernesto.moscoso-externo@unir.net
[c]e-mail: tayyabnaseer48@yahoo.com;tayyab.naseer@khazar.org;tayyab.naseer@math.uol.edu.pk

Despite the extensive previous work carried out in this area of stellar remnants, there are still open physical aspects to be clarified regarding these natural laboratories. For example, we do not fully understand the behavior of matter at densities higher than the atomic nucleus (in the core of a neutron star, for example [43–52]), such as the process that gives rise to the formation of intermediate-mass black holes, such as the process of black hole birth without the appearance of supernovae, among others [53–66]. In particular, the dynamics of the fluids within these compact objects is of great interest. It should be noted that the detailed determination of the coexistence of relativistic fluids inside stellar remnants can be very complex in itself, for many reasons, such as the variability of their nature, the complex ways in which they interact, and, above all, their behaviour under the extreme physical conditions to which they are confined. An intriguing aspect related to such coexistence is the energy interaction between the fluid components inside a stellar compact object, a point that was investigated in [67], where the energy exchange between a polytropic fluid and a generic isotropic fluid was developed based on the use of gravitational decoupling (GD) by extended geometric deformation (MGDe) [68–70]. This approach is highlighted since it permits the study of the energy exchange of the fluid components without resolving the Lane-Emden equation, which does not have analytic solutions. It is possible since this framework solves the problem of EFE for a tensor momentum that is a combination of several sources, that is, $T_{\mu\nu} = T^1_{\mu\nu} + T^2_{\mu\nu} + \cdots + T^n_{\mu\nu}$ in an analytical way. Even the role of each source $T^i_{\mu\nu}$ can be explored, and therefore it is possible to study the total exchange energy between the interior components.

In [67] the well-known Tolman IV solution is considered interacting with a relativistic polytrope where the maximum interaction is presented in the stellar surface with a positive gradient of energy in the radial direction. Subsequently, the energy exchange between the Tolman VII perfect fluid and a polytrope fluid was investigated. In this case such energy exchange is minimum at the centre, having a maximum value at some inner core located around it, and then decreases again towards the surface in contrast to [71]. In both cases, the polytrope fluid releases energy to the environment in order to sustain the static self-gravitating sphere. Thus the framework of GD by MGDe later inspired works such as this, as various aspects of this energy exchange have been studied [72–79]. These studies are vitally important in determining which fluids are most dominant in internal energy exchange and which areas have the most outstanding energy dynamics. It can give us important clues related to the main processes of its evolution and stellar stability. Also, we have to mention that the GD has been widely used in the construction of physically viable models of stellar compact objects [80–98]. This method has even been used recently as a basis for understanding the great influence of the appearance of internal fractures that appear when a compact star system leaves its stellar equilibrium, influencing the energy exchange between relativistic fluids within a compact object (see details in Ref. [99]).

This work seeks to contribute to the understanding of the dynamics of energy exchange within stellar compact objects, specifically in the case of a polytrope with an isotropic fluid type Wyman IIa. For this study, we use the GD by MGDe, taking into account a mimic constraint for the energy density in order to close the generated mathematical problem. The application of the aforementioned method resulted in the use of a numerical approach given the high complexity of the isotropic fluid metric used. Our findings show us that the politrope fluid component plays a fundamental role in the dynamics of energy exchange inside the stellar object. This study is particularly important because it will rigorously analyse the conditions of physical acceptability despite the complexity of the fluid metric.

The present manuscript is organised as follows: In Section 2 we explain the methodology based on gravitational decoupling (GD) by extended minimum geometric deformation (MGDe) to analyse the energy exchange between different gravitational sources; in Section 3 we present the physical acceptability conditions; in Section 4 we describe the analytical development for obtaining the new solution; in Section 5 we present the physical acceptability analysis for this new model; finally, in Section 6 we present conclusions, where we discuss implications and future perspectives.

2 Gravitational decoupling by extended minimal geometric deformation

In this section, we shall briefly review the theoretical framework of GD by MGDe [68–70]. The GD solves the problem of EFE

$$G_{\mu\nu} \equiv R_{\mu\nu} - \frac{1}{2} R g_{\mu\nu} = \kappa T_{\mu\nu}. \tag{1}$$

with

$$T_{\mu\nu} = T^{(s)}_{\mu\nu} + \Theta_{\mu\nu}, \tag{2}$$

where $T^{(s)}_{\mu\nu}$ is known gravitational source, $\Theta_{\mu\nu}$ is an unknown source, and $\kappa = \frac{8\pi G}{c^4}$. At this stage, it is pertinent to elucidate the motivation behind employing the GD approach via MGDe in this study. The

GD framework offers a powerful and systematic method to address the complexity of solving EFE for systems with multiple interacting matter sources, such as the relativistic polytrope and Wyman IIa fluid considered here. By decomposing the total energy-momentum tensor into a known seed source and an additional source , the GD approach allows for the analytical separation of the field equations into manageable subsystems. This decoupling is particularly advantageous in modeling compact stellar objects, where the interplay between different fluid components under extreme gravitational conditions introduces significant mathematical challenges. The MGDe technique enhances this framework by introducing MGD to the metric components, as described in subsequent sections. This method preserves the spherical symmetry of the system while enabling the exploration of anisotropic effects arising from the interaction between the seed and additional sources. Such an approach is crucial for studying energy exchange dynamics, as it provides a tractable pathway to analyze the physical implications of each source's contribution without requiring the direct solution of highly nonlinear equations, such as the Lane-Emden equation for polytropes. Furthermore, the GD approach facilitates the investigation of physically realistic configurations by allowing the imposition of constraints, such as the mimic constraint for energy density used in this work, to close the system of equations. This flexibility makes GD via MGDe an ideal tool for probing the intricate physics of compact stars, offering insights into their stability, structure, and evolutionary processes that are otherwise difficult to obtain through traditional methods.

The effective solution of this problem is a static sphere self-gravitating whose interior space-time is given by

$$ds^2 = e^{\nu}dt^2 - e^{\lambda}dr^2 - r^2 d\Omega^2, \tag{3}$$

where $d\Omega^2 = d\theta^2 + \sin^2\theta d\phi^2$, $\nu(r)$ and $\lambda(r)$ are functions of the radial coordinate r. Thus, we can use this fact, namely, if we use the metric (3) in EFE (1), the effective matter sector of this static sphere is found as:

$$\kappa\rho = \frac{1}{r^2} - e^{-\lambda}\left(\frac{1}{r^2} - \frac{\lambda'}{r}\right), \tag{4}$$

$$\kappa p_r = \frac{1}{r^2} - e^{-\lambda}\left(\frac{1}{r^2} + \frac{\nu'}{r}\right), \tag{5}$$

$$\kappa p_t = -\frac{e^{-\lambda}}{4}\left(2\nu'' + \nu'^2 - \lambda'\nu' + 2\frac{\nu' - \lambda'}{r}\right). \tag{6}$$

These physical quantities are given by:

$$\rho = T_0^{0(s)} + \Theta_0^0, \tag{7}$$

$$p_r = -T_1^{1(s)} - \Theta_1^1, \tag{8}$$

$$p_t = -T_2^{2(s)} - \Theta_2^2, \tag{9}$$

which is the matter sector of an anisotropic fluid static sphere.

Now, it is pertinent to emphasize that GD via MGDe is based in the idea that the seed source $T_{\mu\nu}^{(s)}$ whose space-time:

$$ds^2 = e^{\xi(r)}dt^2 - e^{\mu(r)}dr^2 - r^2 d\Omega^2, \tag{10}$$

is influenced by the extra unknown source $\theta_{\mu\nu}$ in such way its space-time is deformed as:

$$\xi \to v = \xi + g, \tag{11}$$

$$e^{-\mu} \to e^{-\lambda} = e^{-\mu} + f, \tag{12}$$

where f and g are functions only of the radial coordinate, and are known as geometric deformations. It should be noted that these functions must only have dependence on r to maintain the perfect spherical symmetry of the final solution. After, it is crucial to inserts the equations (11)-(12) into (4)-(6), it yields two systems of differential equations:
The first set related to the seed source $T_{\mu\nu}^{(s)}$:

$$\kappa T_0^{0(s)} = \frac{1}{r^2} - e^{-\mu}\left(\frac{1}{r^2} - \frac{\mu'}{r}\right), \tag{13}$$

$$\kappa T_1^{1(s)} = -\frac{1}{r^2} + e^{-\mu}\left(\frac{1}{r^2} + \frac{\xi'}{r}\right), \tag{14}$$

$$\kappa T_2^{2(s)} = \frac{e^{-\mu}}{4}\left(2\xi'' + \xi'^2 - \mu'\xi' + 2\frac{\xi' - \mu'}{r}\right), \tag{15}$$

and the second source-related set $\Theta_{\mu\nu}$:

$$\kappa\Theta_0^0 = -\frac{f}{r^2} - \frac{f'}{r}, \tag{16}$$

$$\kappa\Theta_1^1 - \mathcal{J}_1 = f\left(\frac{1}{r^2} + \frac{\nu'}{r}\right), \tag{17}$$

$$\kappa\Theta_2^2 - \mathcal{J}_2 = \frac{f}{4}\left(2\nu'' + \nu'^2 + 2\frac{\nu'}{r}\right) - \frac{f'}{4}\left(\nu' + \frac{2}{r}\right), \tag{18}$$

where $\mathcal{J}_1 = \frac{e^{-\mu}g'}{r}$ and $4\mathcal{J}_2 = e^{-\mu}\left(2g'' + g'^2 + \frac{2g'}{r} + 2\xi'g' - '\,\mu'g'\right)$.

Precisely the possibility of decoupling the initial problem in these two systems of equations is the key to the success of GD and is what gives this method its name.

Also, it is important to mention that since the Bianchi identities are satisfied by $G_{\mu\nu}$ then

$$\nabla_\mu T^{\mu\nu} = 0, \tag{19}$$

also is satisfied. Thus, using the energy-momentum tensor (2) into (19), we obtain (see the calculation details in [67]):

$$\nabla_\sigma T^{\sigma(s)}_\nu = -\nabla_\sigma \Theta^\sigma_\nu = -\frac{g'}{2}\left(T^{0(s)}_0 - T^{1(s)}_1\right)\delta^\sigma_\nu. \tag{20}$$

The above equation has a prominent importance given that it determines the energy interchange between the relativistic fluids $\{T^{(s)}_{\mu\nu}, \Theta_{\mu,\nu}\}$ that sustain the self-gravitating sphere; indeed, it gives us:

$$\Delta E = \frac{g'}{2\kappa}\frac{e^{-\mu}}{r}(\xi' + \mu'), \tag{21}$$

where, if $g' > 0$ implies that $\Delta E > 0$, that is, the source $\Theta_{\mu\nu}$ releases energy to the environment, while if $g' < 0$, then $T^{(s)}_{\mu\nu}$ is the one that provides its energy so that the two fluids can coexist within the self-gravitating sphere. This result is too important, since it permits modeling the energy interaction between the fluids that support a self-gravitating sphere.

Specifically, the above development is a precursor to the possibility of studying the energy exchange between relativistic fluids that form a compact stellar object. These studies have already been mentioned above. Thus, our objective is to use this method, together with the one developed in [67], to study the possibility of having realistic compact stellar configurations supported by two stellar fluids, such as the isotropic Wyman IIa fluid ($n = 1$) and a relativistic polytropic fluid, and to examine the dynamics of the energy exchange between them.

But before constructing this effective model, let's review a little about the relativistic fluids that support it, as well as the conditions of physical acceptability that our effective model must meet.

2.1 Wyman IIa isotropic fluid

For this research we used as a known source $T^{(s)}_{\mu\nu}$ the Wyman IIa solution (with $n = 1$), which is an isotropic stellar fluid whose metric is [7, 100]:

$$e^{\xi} = (A - Br^2)^2, \tag{22}$$

$$e^{-\mu} = 1 + Cr^2(A - 3Br^2)^{-\frac{2}{3}}, \tag{23}$$

where A is a dimensionless constant, while B and C are constants with dimensions inverse to the length squared. The selection of such a fluid as the seed source in this study is driven by its well-established physical properties and its applicability within the framework of general relativity for modeling compact stellar objects. The Wyman IIa solution, characterized by its isotropic pressure profile and analytical tractability, provides a robust foundation for studying complex relativistic systems. Its metric offers a mathematically consistent and physically realistic description of a self-gravitating sphere, making it an ideal candidate for exploring energy interactions with a relativistic polytrope. Furthermore, the Wyman IIa fluid's prior successful application in gravitational decoupling studies, underscores its versatility in generating new stellar models. By choosing this fluid, we ensure a reliable starting point that facilitates the analytical and numerical exploration of energy exchange dynamics while maintaining compatibility with the physical acceptability conditions required for realistic compact star configurations. This choice also allows for a direct comparison with previous studies involving other isotropic fluids, such as Tolman IV and Tolman VII, thereby contributing to a broader understanding of fluid interactions in stellar remnants.

The matter sector of this interior solution is

$$T^{0(s)}_0 = \rho^{(s)} = \frac{(5Br^2 - 3A)\,C}{\kappa\,(A - 3Br^2)^{5/3}}, \tag{24}$$

$$T^{1(s)}_1 = T^{2(s)}_2 = T^{3(s)}_3 = p^{(s)} = \frac{\left(5 - \frac{4A}{A - Br^2}\right)\left(\frac{Cr^2}{(A - 3Br^2)^{2/3}} + 1\right) - 1}{\kappa r^2} \tag{25}$$

This solution has previously been used as a seed solution within the GD method for the purpose of finding new stellar models in [101–103]. This is why we chose this seed, which does not preclude working with other seed solutions in future works.

2.2 Polytrope

Now, the unknown source $\Theta_{\mu\nu}$ is considered as a relativistic polytrope whose equation of state can be written as

$$P_r = K\rho^{\Gamma}_\Theta = K\rho^{1+\frac{1}{n}}_\Theta, \tag{26}$$

where P_r is the isotropic pressure and ρ_Θ is the (baryonic) mass density. The constants K, Γ, and n are usually referred to as the polytropic constant, polytropic exponent, and polytropic index, respectively. From the above, we know that this equation of state will only depend on the pressure, $\rho_\Theta = \rho_\Theta(P_r)$ [18]. When the constant K is calculated from natural constants, the polytropic equation of state can be used to model a non-relativistic, completely degenerate Fermi gas ($n = 5/3$), and in the relativistic limit ($n = 4/3$). Otherwise, if K is a free parameter, the models can be used to describe an isothermal ideal gas or a completely convective star. Polytropes are also known to play an important role in

the study of stellar structures for several fundamental astrophysical problems. For example, objects such as anisotropic white dwarfs have been modelled considering a general formalism to study Newtonian polytropes for anisotropic matter [**?**, 104, 105].

Furthermore, this choice is particularly advantageous in the context of MGDe, as it simplifies the analytical treatment of the energy-momentum tensor for the additional source. The polytropic model facilitates the exploration of energy exchange dynamics between the relativistic polytrope and the isotropic Wyman IIa fluid, enabling a tractable analysis of their interaction without the need to solve the complex Lane-Emden equation numerically. Furthermore, the polytropic equation of state is well-suited for studying the stability and structural properties of compact objects, as it accounts for the effects of high-density environments and anisotropic pressures, which are critical for understanding the physical realism of the resulting stellar configurations. This approach aligns with established astrophysical models and provides a robust foundation for investigating the intricate interplay of relativistic fluids within self-gravitating systems. Note that that we have used the subscript Θ in Eq. (26) to avoid confusion with the total density of the effective system in our work.

3 Physical acceptability conditions

Every anisotropic interior solution must meet a set of physical acceptability conditions in order to model a realistic compact star. These are detailed in [107]:

1. **Regular space - time**
   The spacetime metric components of the interior solution are positive functions; they must be finite and free of singularities inside the star. At the centre, they must satisfy $e^{-\lambda(0)} = 1$ and $e^{\nu(0)} = constant$. Furthermore, $e^{-\lambda}$ is a monotonically decreasing function and e^{ν} is monotonically increasing.
2. **Matching conditions**
   On the surface of the star $r = R$ the interior solution must coincide with the exterior Schwarzschild solution, which determines that:
   $$e^{\nu(r=R)} = e^{-\lambda(r=R)} = 1 - \frac{2M}{R}, \tag{27}$$
   where R is the radius of the star and M its total mass.
   Likewise, the radial pressure at this point disappears
   $$p_r(r = R) = 0, \tag{28}$$
   because there is emptiness outside the compact star.
3. **Causality condition**
   The radial velocity $v_r^2 = \frac{dp_r}{d\rho}$ and tangential velocity $v_t^2 = \frac{dp_t}{d\rho}$ of sound inside the stellar object must not exceed the causal limit of the speed of light ($c = 1$); therefore:
   $$0 \leq v_r^2 < 1 \quad \text{and} \quad 0 \leq v_t^2 < 1. \tag{29}$$
4. **Matter sector**
   The quantities ρ, p_r, p_t must be positive, monotonically decreasing, and continuous functions. Furthermore, they reach their maximum at the centre, that is, $\rho'(0) = p_r'(0) = p_t'(0) = 0$. The tangential pressure must remain greater than the radial pressure inside the star, with the exception of the centre, where $p_t(0) = p_r(0)$.
5. **Energy conditions**
   The material sector of the solution must satisfy the dominant energy condition (DEC):
   $$\rho \geq p_r, \quad \text{and} \quad \rho \geq p_t. \tag{30}$$
   It is desirable but not mandatory that the strong energy condition (SEC):
   $$\rho \geq p_r + 2p_t, \tag{31}$$
   be fulfilled.
6. **Redshift**
   The redshift function $Z(r) = \frac{1}{\sqrt{e^{\nu}}} - 1$ must be continuous and positive, decreasing with the radial variable r. Its value on the surface $Z(r = R)$ has to be less than the universal limit $Z_{\text{bound}} = 5.211$. And if the solution satisfies the SEC, then the limit is $Z_{\text{bound}} = 3.842$ [108, 109].

Now with all this shown above, we show below the construction of our effective compact stellar model.

4 Effective stellar model

First of all, to build our effective interior solution, we will remember that the resulting self-gravitating sphere is composed of two relativistic fluids: one, the seed source $T_{\mu\nu}$ given by

$$T_{\nu}^{\mu(s)} = diag[\rho^{(s)}, -p_r^{(s)}, -p_t^{(s)}, -p_t^{(s)}], \tag{32}$$

which we consider the Wyman IIa fluid; and the other source $\Theta_{\mu\nu}$ is given an isotropic politrope whose matter sector is given by

$$\theta_{\nu}^{\mu} = diag[\rho_{\Theta}, -P_r, -P_r, -P_r]. \tag{33}$$

After, we will use the mimic constraint for the energy density

$$\rho_{\Theta} \sim \rho^{(s)}, \tag{34}$$

in order to study the energy interaction between these fluids with the help of the GD by MGDe approach.

In fact, we use the method developed in [67], where two ways are proposed: one is the aforementioned mimic constraint for energy density and the other is the mimic constraint for pressure. We check both ways for our case, and the way described by the mimic pressure constraint results in a non-viable result because of the difficulties in calculations.

Now, the most simple expression that satisfies (34) is:

$$\rho_{\Theta}(r) = \alpha(K,\Gamma)\rho^{(s)}, \tag{35}$$

where we use a new quantity $\alpha(K,\Gamma)$, which is consistent with the polytrope equation, (26), and with the condition $f(r)|_{K=0} = 0$, which is expressed as follows:

$$\alpha(K,\Gamma) = K^{\Gamma}. \tag{36}$$

Precisely, using the Eq. (35) in EFE (13)-(18), the following differential equation emerges:

$$\frac{f'(r)}{r} + \frac{f(r)}{r^2} = -K^{\Gamma}\left[\frac{1}{r^2} - e^{-\mu(r)}\left(\frac{1}{r^2} - \frac{\mu'(r)}{r}\right)\right] \tag{37}$$

This above differential equation is resolved using the metric component (23), which yields

$$f = \frac{CK^{1+\frac{1}{n}}\, r^2}{(A - 3Br^2)^{\frac{2}{3}}}. \tag{38}$$

Thus, the deformation function f has been found; the next step is to find the function g. To do this, we calculate first $g'(r)$ through the polytrope equation (26) and Eq. (35), giving us:

$$P_r = K(K^{\Gamma}\rho^{(s)})^{\Gamma}. \tag{39}$$

Then using the EFE (13)-(18), which results in

$$g' = \frac{r}{e^{-\mu} + f}\left[\kappa K\left(\frac{(K)^{\Gamma}}{\kappa}\left(\frac{1}{r^2} - e^{-\mu}\left(\frac{1}{r^2} - \frac{\mu'}{r}\right)\right)\right)^{\Gamma} - f\left(\frac{1}{r^2} + \frac{\xi'}{r}\right)\right]. \tag{40}$$

This previous expression is easy to find explicitly with the help of the equations (23) and (38), thus we have:

$$g' = \frac{r}{1 + \frac{C\left(1+K^{1+\frac{1}{n}}\right)r^2}{(A-3Br^2)^{\frac{2}{3}}}}\left[-\frac{CK^{1+\frac{1}{n}}(A - 5Br^2)}{(A - 3Br^2)^{\frac{2}{3}}(A - Br^2)} + K\left(-\frac{CK^{1+\frac{1}{n}}(3A - 5Br^2)}{(A - 3Br^2)^{\frac{5}{3}}\kappa}\right)^{1+\frac{1}{n}}\kappa\right] \tag{41}$$

At this point it is worth emphasising that it is true that with only the information of g' one can find the effective material sector given by the field equations (4)-(6), since they depend only on ν' and not on ν (see equations (11)-(12)); but in this work we want to go a step further than previous works in which the effective material sector is studied, but the effective space-time is neglected, which seems very important to us when ensuring the plausibility of our model in its entirety. Thus, if we are going to calculate g, even if it is numerically given the difficulty of integrating the expression of g'.

To obtain g, we use the variable change of $r \to xR$ to work in units of star radius, so we consider an integration interval of $[0,1]$. Therefore, the g function can be written as

$$g = \int_0^1 \left[\frac{R^2 x}{1 + \frac{C\left(1+K^{1+\frac{1}{n}}\right)R^2x^2}{(A-3BR^2x^2)^{\frac{2}{3}}}}\right] \times \left[-\frac{CK^{1+\frac{1}{n}}(A - 5BR^2x^2)}{(A - 3BR^2x^2)^{\frac{2}{3}}(A - BR^2x^2)} + K\left(-\frac{CK^{1+\frac{1}{n}}(3A - 5BR^2x^2)}{(A - 3BR^2x^2)^{\frac{5}{3}}\kappa}\right)^{1+\frac{1}{n}}\kappa\right]\mathrm{d}x. \tag{42}$$

To evaluate the integral involved in the model, once values were assigned to the free parameters $[A, B, C, K, R, n, \kappa]$, we employed the *global adaptive quadrature method* proposed by Gander and Gautschi [110]. This algorithm is particularly suitable for integrands that present peaks, steep gradients, or complicated behaviour within the integration interval.

The method is based on the systematic subdivision of the integration domain into smaller subintervals, where high-order quadrature rules are applied. The algorithm adaptively refines those subintervals in which the local error estimate exceeds a prescribed tolerance, thereby ensuring an efficient allocation of evaluation points. Unlike local refinement strategies, the global adaptive approach provides control of the error across the entire interval, which guarantees both robustness and accuracy.

This strategy is especially advantageous in relativistic stellar models, where the integrands often display singular-like features or rapid variations near the stellar surface. By applying the Gander–Gautschi algorithm, it is possible to obtain a reliable and precise evaluation of the integrals without requiring an a priori regularization of the integrand, making it a natural choice for this class of problems.

4.1 Effective space-time

Now, let's find the physical quantities that represent our model. Thus, in order to obtain the effective space-time, we use the Eq. (37) and (23) in (12) resulting in:

$$e^{\lambda}=1+\frac{C(1+K^{1+1/n})r^2}{(A-3Br^2)^{2/3}}. \tag{43}$$

Respect for the temporal metric component is found using Eq. (41) in Eq. (23), and taking into account the fact that $\nu'=\xi'+g'$, we obtain

$$\begin{aligned}\nu'=&-\frac{4Br}{A-Br^2}+\frac{r}{1+\frac{C(1+K^{1+\frac{1}{n}})r^2}{(A-3Br^2)^{\frac{2}{3}}}}\times\\&\left[-\frac{C\,K^{1+\frac{1}{n}}(A-5Br^2)}{(A-3Br^2)^{\frac{2}{3}}(A-Br^2)}\right.\\&\left.+K\left(-\frac{C\,K^{1+\frac{1}{n}}(3A-5Br^2)}{(A-3Br^2)^{\frac{5}{3}}\kappa}\right)^{1+\frac{1}{n}}\kappa\right].\end{aligned} \tag{44}$$

Now as we found the value of g numerically, then the value of ν is found as

$$\nu=\xi+g=\ln(A-Br^2)^2+g, \tag{45}$$

namely

$$e^{\nu}=c_1\left(A-BR^2\right)^2, \tag{46}$$

where c_1 represents a constant that varies according to the numerical value of the integral given by Eq. (42).

4.2 New matter sector

As for the effective material sector, this is found by using (43) and (44) into the EFE (4)-(6). Hence, we find:

$$\rho=-\frac{C\left(K^{\frac{1}{n}+1}+1\right)(3A-5Br^2)}{\kappa\,(A-3Br^2)^{5/3}}, \tag{47}$$

$$\begin{aligned}p_r=&\frac{\kappa\,K\,(A-Br^2)(A-3Br^2)}{\kappa(A-3Br^2)(A-Br^2)}\times\\&\left(-\frac{CK^{\frac{1}{n}+1}(3A-5Br^2)}{\kappa(A-3Br^2)^{5/3}}\right)^{\frac{1}{n}+1}\\&+\frac{C(A-5Br^2)\sqrt[3]{A-3Br^2}}{\kappa(A-3Br^2)(A-Br^2)}\\&+\frac{-4AB+12B^2r^2}{\kappa(A-3Br^2)(A-Br^2)}.\end{aligned} \tag{48}$$

$$\begin{aligned}p_t=&\frac{1}{4\,(A-3Br^2)^{8/3}}\left[\frac{20BCr^2\left(A-3Br^2\right)^2}{A-Br^2}\times\right.\\&K^{1+\frac{1}{n}}\\&+\frac{4BCr^2\left(A-3Br^2\right)^2(A-5Br^2)\,K^{1+\frac{1}{n}}}{(A-Br^2)^2}\\&-\frac{4C\,(A-5Br^2)\left(A-3Br^2\right)^2K^{1+\frac{1}{n}}}{A-Br^2}\\&-\frac{8BCr^2\,(A-5Br^2)\left(A-3Br^2\right)K^{1+\frac{1}{n}}}{A-Br^2}\\&+\frac{2C^2\left(K^{1+\frac{1}{n}}+1\right)r^2\left(A-3Br^2\right)}{(A-3Br^2)^{2/3}+C\left(K^{1+\frac{1}{n}}+1\right)r^2}\times\\&(A-5Br^2)\,K^{1+\frac{1}{n}}\\&+\frac{C^2r^2\left(A-3Br^2\right)^2(A-5Br^2)^2K^{2+\frac{2}{n}}}{(A-Br^2)^2}\\&\left((A-3Br^2)^{2/3}+C\left(K^{1+\frac{1}{n}}+1\right)r^2\right)^{-1}\\&+\frac{C^2r^2\left(3A-5Br^2\right)^2}{(A-3Br^2)^{2/3}+C\left(K^{1+\frac{1}{n}}+1\right)r^2}\times\\&\left(-\frac{CK^{1+\frac{1}{n}}\left(3A-5Br^2\right)}{(A-3Br^2)^{5/3}\,\kappa}\right)^{2/n}K^{4+\frac{2}{n}}\\&-8BC\left(K^{1+\frac{1}{n}}+1\right)r^2\left(A-3Br^2\right)\\&+4C\left(K^{1+\frac{1}{n}}+1\right)(A-Br^2)\left(A-3Br^2\right)\\&-\frac{16B\left(A-3Br^2\right)^2}{A-Br^2}\times\\&\left((A-3Br^2)^{2/3}+C\left(K^{1+\frac{1}{n}}+1\right)r^2\right)\\&-\frac{2CK^{2+\frac{1}{n}}}{n\,(A-Br^2)}\times\\&\left((A-3Br^2)^{2/3}+C\left(K^{1+\frac{1}{n}}+1\right)r^2\right)^{-1}\\&\left.\chi(r)\left(-\frac{CK^{1+\frac{1}{n}}\left(3A-5Br^2\right)}{(A-3Br^2)^{5/3}\,\kappa}\right)^{1/n}\right],\end{aligned} \tag{49}$$

with

$$\begin{aligned}\chi=&\,5B^3\Big(2(2-7n)\left(A-3Br^2\right)^{2/3}\\&+C\left(2(n+2)K^{1+\frac{1}{n}}-13n+4\right)r^2\Big)r^6\\&+AB^2\Big(2(37n-20)\left(A-3Br^2\right)^{2/3}\\&+C\left(-8(3n+5)K^{1+\frac{1}{n}}+61n-40\right)r^2\Big)r^4\\&+A^2B\Big(2(10-13n)\left(A-3Br^2\right)^{2/3}\end{aligned}$$

$$+C\left(2(7n+10)K^{1+\frac{1}{n}}-15n+20\right)r^2\Bigg)r^2$$
$$+3A^3n\left(2\left(A-3Br^2\right)^{2/3}+Cr^2\right) \quad (50)$$

Using the matching conditions (27) with (43) and (46), we then obtain the following relations:

$$A=BR^2+\sqrt{\frac{R-2M}{c_1R}}, \quad (51)$$

$$C=-\frac{2M\left(A-3BR^2\right)^{2/3}}{R^3\left(\mathrm{K}^{\frac{1}{n}+1}+1\right)}. \quad (52)$$

where the constant c_1 depends on the integration of Eq. (42).

On the other hand, if we try to apply the condition (28) in p_r given by Eq. (48) analytically becomes complex issue. This difficulty was raised through a numerical treatment that focuses on obtaining a compactness factor $u=\frac{M}{R}$ such that this condition is met. To do this, in the equation (48), we use the change of variables $M\to uR, r\to xR$, which results in an equation that no longer depends on r. In this way, by evaluating R and x as one (in units of the stellar radius), we managed to obtain an equation that can be solved for u. This procedure was necessary to obtain realistic behaviour of our model.

5 Results

In this part, we analyze first the physical acceptability of the stellar model and then the energy exchange between the fluids that compose the self-gravitating sphere that represents such a model. We checked that the model behaves well with $B=0.45$ with the restriction (52) and the restriction given by Eq. (51), where the parameter c_1 is determined by Eq. (42), and also behaves very regularly for the polytropic index of $n=0.5$. Therefore, our model is precisely the interior of a stellar compact object that is supported by an isotropic fluid type Wyman IIa ($n=1$) and a politrope that is typical in the interior of a neutron star [**?**]. Thus, we have a compact object with a very exotic interior.

We reviewed that finding configurations that satisfy all the conditions of physical acceptability was not an easy task; in fact, small variations in the parameters give physically unrealistic results. In this sense, we have focused on the following configurations for the physical analysis of the model: $K=0.43$ with $u=0.302917$, which is shown in all figures below in the black line, $K=0.44$ with $u=0.334079$ (in the blue line) and $K=0.47$ with $u=0.176426$ (in the red line).

5.1 Acceptability physical analysis

5.1.1 Matter sector

We first plot the profile of the matter sector $\{\rho, p_r, p_t\}$ in Figs. 1, 2, and 3. We observed that these physical quantities have their maximum values at the centre of the star. They also are positive, continuous, and monotonously decreasing functions of the radial variable r. Moreover, in Fig. 2 we can observe that Eq. (28) is satisfied. Also, the local anisotropy function $\Pi=p_t-p_r$ is positive. This grows as one approaches the radius of the star from the centre (see Fig. 4). Furthermore, we can notice that at the center of the star the anisotropy is zero so there is no collapse and the core of the star tends towards stability. Thus, we have confirmed the physical acceptability of the material sector of our model.

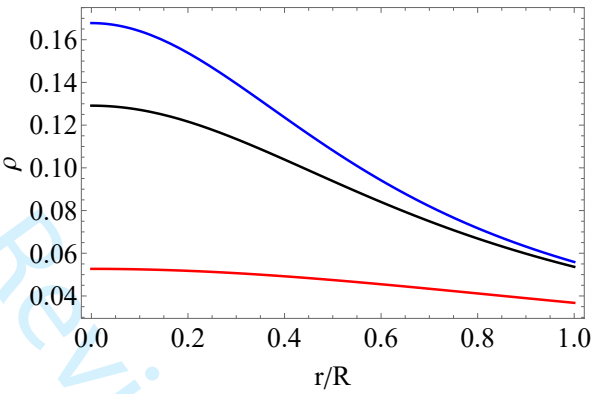

Fig. 1: Energy density profiles

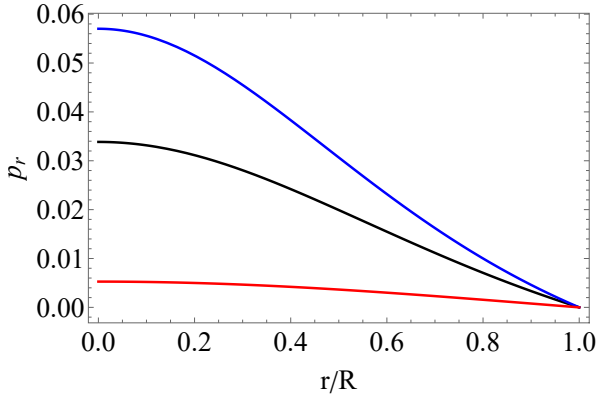

Fig. 2: Radial pressure profiles

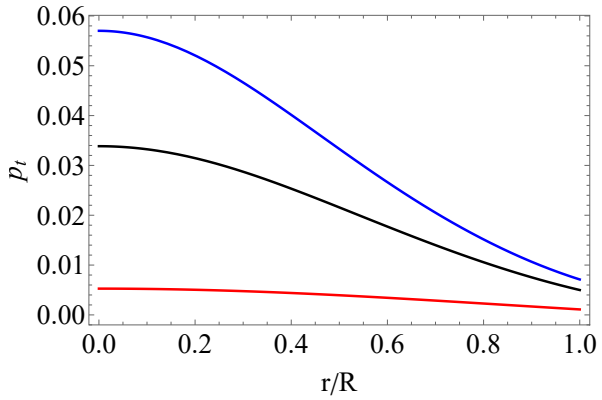

Fig. 3: Tangential pressure profiles

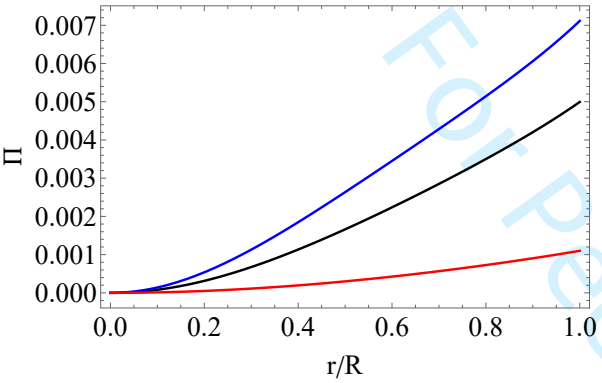

Fig. 4: Anisotropy in pressure profiles

5.1.2 New interior space-time

The spacetime metric components of the interior solution are positive and finite functions. In the centre, the radial metric satisfies $e^{-\lambda(0)} = 1$ and is monotonically decreasing of r (see Fig. 5). While e^{ν} is a monotonously decreasing function of the same variable r and $e^{\nu(0)} =$ constant (see Fig. 6).

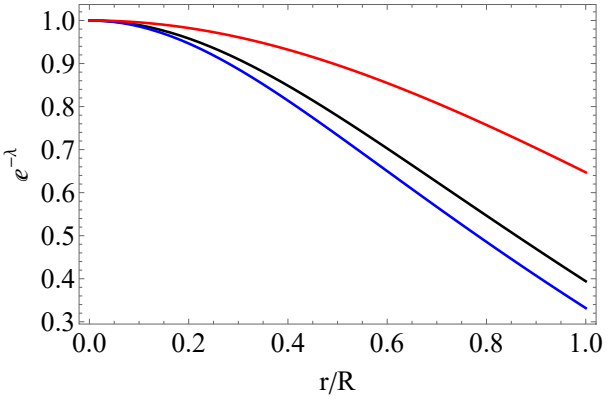

Fig. 5: Radial component of the metric profile

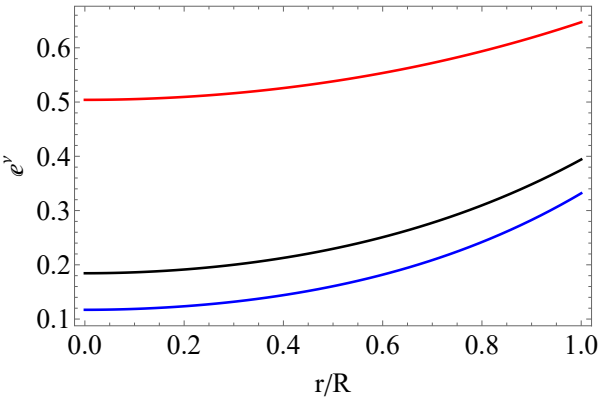

Fig. 6: Temporal component of the metric profile

5.1.3 Energy conditions

In Figs. 7 and 8, we observe that the dominant energy condition given by Eq. (30) is satisfied. Furthermore, in Fig.9, we can observe that the strong energy condition given by Eq. (31) is satisfied for $K = 0.43$ with $u = 0.302917$ (black line) and $K = 0.47$ with $u = 0.176426$ (red line) configurations; this indicates that the model is physically viable. In contrast, for $K = 0.44$ with $u = 0.334079$ (blue line), the SEC is violated, suggesting that this model can be unstable for such a configuration. According to [111], SEC violation can occur in systems with negative pressures or extreme conditions, such as in certain neutron star models.

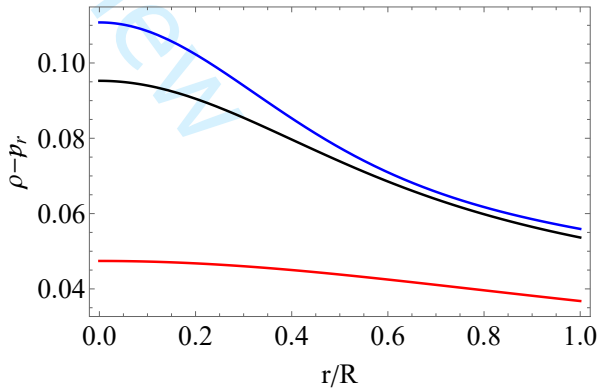

Fig. 7: $\rho - p_r$ profile

5.1.4 Redshift function

In Fig. 10, we notice that Z is positive and is a monotonically decreasing function of the radial variable r. We also see that for the models that comply with the

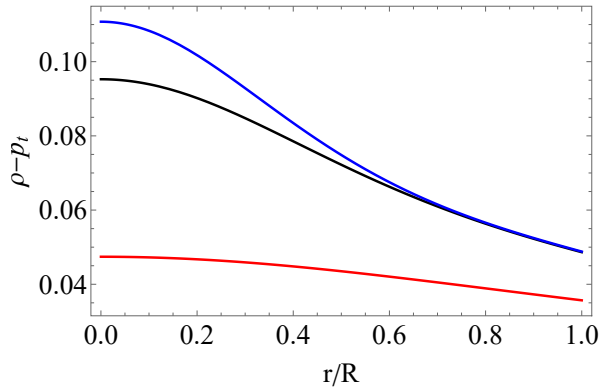

Fig. 8: $\rho - p_t$ profile

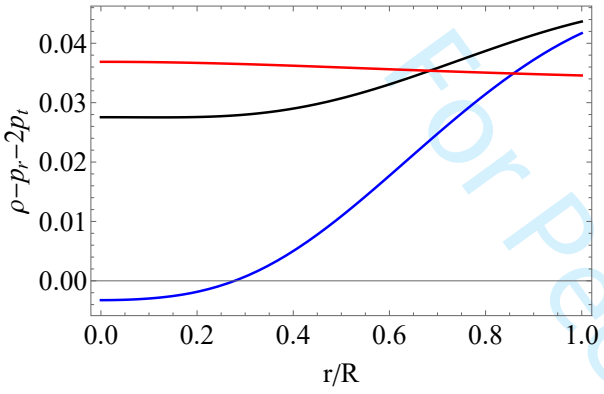

Fig. 9: $\rho - p_r - 2p_t$ profile

SEC (see illustration 9), $K = 0.44$ and $K = 0.47$, and the value on the surface is less than 3.842, fulfilling the acceptability condition 6. While for model $K = 0.43$, since it does not comply with the SEC, it must have a value less than the universal limit of 5.211 on the stellar surface. In fact, this value is $Z = 0.735938$, also fulfilling the mentioned condition.

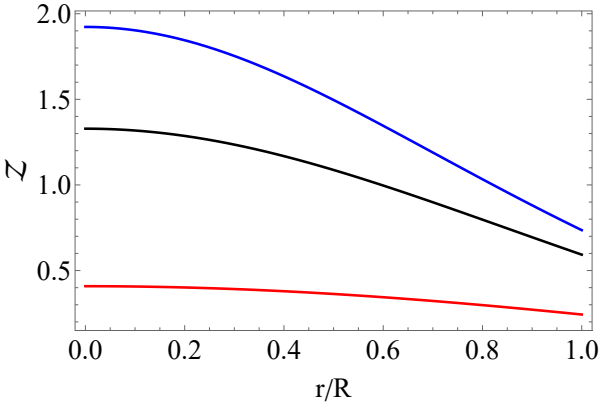

Fig. 10: Redshift function profile

5.1.5 Causality condition

To satisfy this condition, the relationships given by Eq. (29) must be met. We can observe that in Figs. 11 and 12, this condition is indeed fulfilled. This shows that the model meets the causality condition, because the radial velocity v_r^2 and the tangential velocity v_t^2 of sound inside the stellar object do not exceed the causal limit of the speed of light $c = 1$. It is important to note that since these interior sound velocity profiles are not monotonously decreasing functions of the radial variable r, it is possible that the model may have some instability.

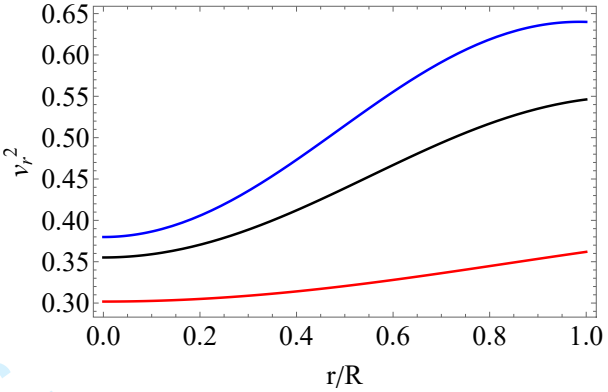

Fig. 11: Radial sound velocity profile

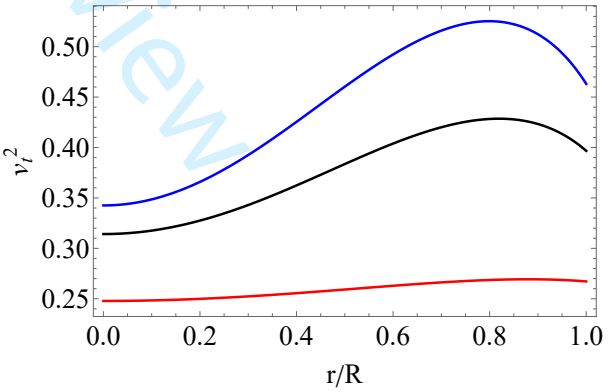

Fig. 12: Tangential sound velocity profile

Before analysing the energy exchange within the stellar compact object modelled by our new interior solution, we see from all this previous analysis that it is physically realistic since it meets all the conditions of physical acceptability for a self-gravitating sphere supported by an anisotropic fluid, at least for the configurations analysed previously.

5.2 Energy exchange between both relativistic fluids

We show the behaviour of ΔE given by Eq. (21) in Fig. 13, namely, the energy interchange between both fluids: the Wyman IIa ($n = 1$) isotropic fluid and the polytrope. It is shown that $\Delta E > 0$, and these interchanges increase for the outer regions of the stellar compact object for the configurations that we considered. Therefore, it can be deduced that the polytrope transfers energy to the environment to achieve coexistence with the perfect fluid within the resulting stellar object. On the other hand, in the stellar centre the energy exchange is null ($\Delta E = 0$), which indicates stability in that region, and this energy exchange increases as the r moves to more external areas of the compact star.

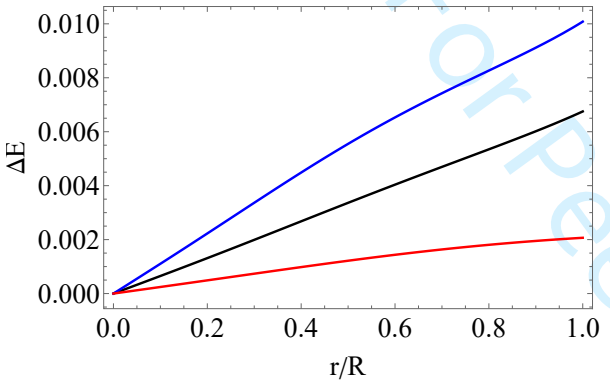

Fig. 13: Energy interchange profile

In Fig. 14, the energy exchange is shown for three values of compactness factors u with fixed $K = 0.43$. This interchange is more elevated for the more compact configurations. Instead, in Fig. 15, the energy exchange is shown for $u = 0.3340$ and three different values of K. We observe that the intensity of the energy exchange is increased as K increases. Therefore, the intensity of the energy exchange between relativistic fluids is favoured with the increase in the value of K and of the compactness factor.

6 Conclusions and remarks

The energetic interaction between two relativistic fluids was analysed, one consisting of an isotropic relativistic polytrope and the other a Wymann IIa-type isotropic fluid, forming a realistic stellar compact object. This was made possible by using the GD via the MGDe framework. Precisely, the seed source considered was a well-known Wymann IIa fluid (with $n = 1$), and the extra source $\Theta_{\mu\nu}$ is a polytrope, and using the algorithm developed in [67] with the use of mimic constraint for energy density, namely, assuming that the energy densities between the interacting fluids are the same, which allowed to found the function g' given by Eq. (41). After that, the numerical integration of g' was carried out, in which values were taken for the different constants involved such as A, B, K, n, so that the stellar model meets all the conditions of physical acceptability for an anisotropic compact star. It is true that one can calculate the material sector of the stellar model only with the value of g' since the EFE depends on ν' and not on ν, but we set out to find real values of g and ν since we also wanted to ensure a physically realistic interior space-time. As a result, three exotic configurations were generated, all consistent with the physical acceptability criteria. However, only two of these configurations fully met the Strong Energy Condition (see Eq. (31)). We checked that for the set of values of $[-1.638; -3.121]$ for g the model is physically viable.

It is importan to mention, that the possibility of using a mimic constraint for the pressure was also viable; however, this did not yield physically realistic results. This does not mean that other types of constraints can be explored to conduct this type of study; the task is not at all easy, but it would be very interesting.

As a main result, we found that for the system to be physically realistic, it is necessary for the polytrope to deliver energy to the environment. Precisely, in the case when a Tolman IV fluid interacts with the polytrope also has the same direction of energy exchange [67], that is, the polytrope releases the energy in order to sostain the self-gravitating sphere compatible with the exterior solution of Schwarzschild. Same thing was also reported in [71], namely, that is necesary the exchange energy is from the polytrope (in such case the isotropic fluid used was the Tolman VII). Thus, we have three coincidencies respect the direction in which a perfect fluid interacts energetically with a relativistic polytrope inside an stellar compact object. It can be thinking the polytrope does a work in order to mantain the fluid polytrope in the interior of the compact star. In a sense, a similar study could be done with another isotropic fluid to be able to answer more precisely whether this direction in which this exchange occurs is the same regardless of the isotropic solution chosen. This task is not at all easy, but it is worth doing since it will answer this question, which we believe, with three coincidences already shown in a hundred ways, already tells us a lot about a certain trend.

Now, the exchange energy in our case is zero in the centre of the stellar object and increases for the outermost regions of the astrophysical object. This behaviour is the same for the Tolman IV case, and it is different

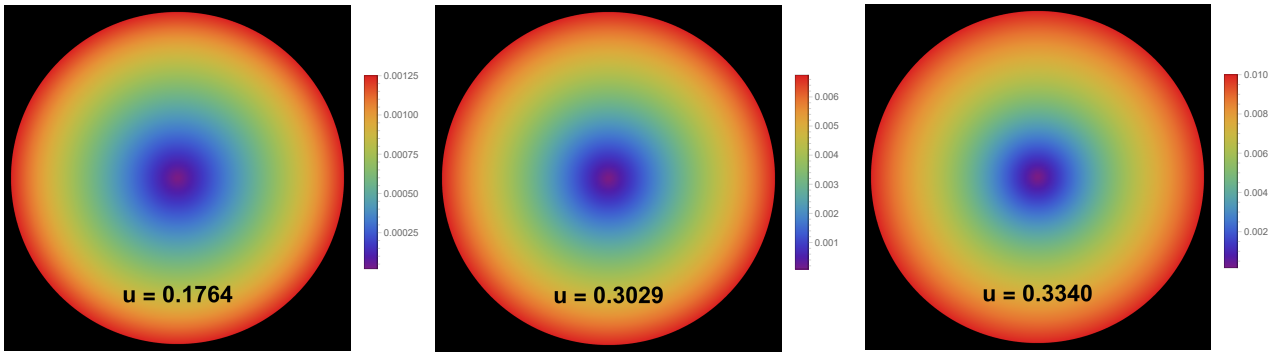

Fig. 14: ΔE density plot for $K = 0.43$ and a) with $u = 0.1764$, b) with $u = 0.3029$, and c) with $u = 0.3340$.

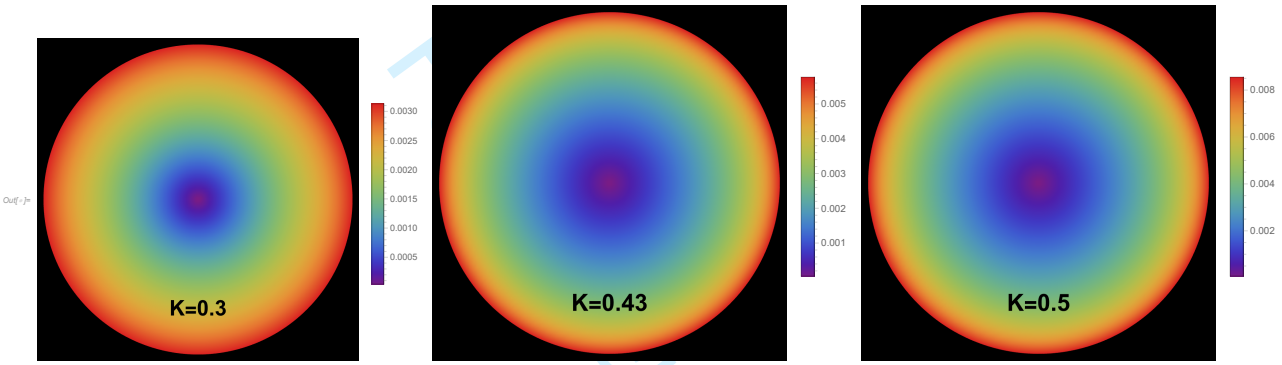

Fig. 15: ΔE density plot for the compactness factor of $u = 0.3340$ with a) $K = 0.30$, b) $K = 0.43$, and c) $K = 0.50$.

in the case of Tolman VII, but the three cases coincides in the fact the energy exchange is null in the centre of the compact star, which suggest it is a mandatory characteristic of these objects. Moreover, we that the energy exchange is more intense for increasingly compact stars and as the values of the constant K increase in our case. It is also important to highlight the possible relationship that anisotropy has with energy exchange; precisely, this is zero in the centre, which may be related to the suppression of energy exchange ($\Delta E = 0$) inside the stellar object. However, in more external areas, the interactions increase, generating anisotropy and consequently an energy exchange. In fact, we have verified that those configurations that do not satisfy the SEC condition have wider external regions than those that do, so that the presence of wider energy exchange zones in some ways accounts for more unstable configurations. This contrast underscores the critical role of the SEC in regulating energy interactions within complex relativistic systems.

We have to emphatize the importance of this work and the mentioned in the above paragraph since the study of the polytropes in general relativity is not an easy task since one have to solve numerically the Lane–Emden equations. But with the help of the framework of GD via MGDe such difficulty is avoided in order to study the energy exchange between the fluids that supports a stellar compact object. The way to do it in the case of the isotropic fluid and polytrope was developed by [67] via two mimic constraints is not easy task, also is necessary a numerical approach. We believe that is necessary to carry out investigations about the stability of these compact objects, namely, using diverse criteria of stability. Specifically, can be very worth the study of such objects under radial and non-radial perturbations. It may even be very ambitious to carry out a study on the influence of gravitational cracking on the exchange of both fluids, as has already been done for a specific case in [99]. Clearly, all these types of studies will contribute enormously to our understanding of the physics within stellar remnants, both in their evolution and in their most relevant events.

To further advance the understanding of energy exchange dynamics within compact stellar objects, future research could explore alternative isotropic fluid models interacting with polytropic fluids to determine if

the observed energy transfer trends are universal across different fluid configurations. Investigating the impact of varying polytropic indices and compactness factors on energy exchange could provide deeper insights into the stability and evolution of these systems. Additionally, incorporating non-radial perturbations and gravitational cracking analyses could reveal how structural instabilities influence fluid interactions, potentially uncovering new mechanisms driving stellar evolution. Extending the gravitational decoupling framework to include multi-fluid systems or anisotropic seed solutions may also yield novel stellar models, enhancing our understanding of complex astrophysical phenomena. Finally, leveraging advanced numerical techniques, such as machine learning-driven simulations, could improve the precision of modeling energy exchanges, offering a pathway to explore extreme conditions within stellar remnants.

References

1. A. Einstein, Die Feldgleichungen der Gravitation. Sitzungsber. Königl. Preuss. Akad. Wiss. Berlin (Math. Phys.), 1915, 844–847
2. A. Einstein, Die Feldgleichungen der Gravitation. Sitzungsber. Königl. Preuss. Akad. Wiss. Berlin (Math. Phys.), 1915, 844–847
3. K. Schwarzschild, On the gravitational field of a sphere of incompressible fluid according to Einstein's theory. arXiv:physics/9912033 (1999)
4. K. Schwarzschild, On the gravitational field of a mass point according to Einstein's theory. arXiv:physics/9905030 (1999)
5. R.C. Tolman, Static solutions of einstein's field equations for spheres of fluid. Phys. Rev. **55**(4), 364 (1939)
6. J.R. Oppenheimer, G.M. Volkoff, On massive neutron cores. Phys. Rev. **55**(4), 374 (1939)
7. M. Delgaty, K. Lake, Physical acceptability of isolated, static, spherically symmetric, perfect fluid solutions of Einstein's equations. Comput. Phys. Commun. **115**, 395–415 (1998)
8. M.R. Finch, J.E. Skea, A realistic stellar model based on an ansatz of Duorah and Ray. Class. Quantum Grav. **6**, 467 (1989)
9. B. Ivanov, Static charged perfect fluid spheres in general relativity. Phys. Rev. D **65**(10), 104001 (2002)
10. M.H. Murad, N. Pant, A class of exact isotropic solutions of Einstein's equations and relativistic stellar models in general relativity. Astrophys. Space Sci. **350**, 349–359 (2014)
11. J. Kumar & P. Bharti, An isotropic compact stellar model in curvature coordinate system consistent with observational data. Eur. Phys. J. Plus, bf 137(3), 330 (2022)
12. M.K. Mak and T. Harko, Isotropic stars in general relativity. Eur. Phys. J. C **73**(10), 2585 (2013)
13. G.G.L. Nashed, Isotropic stellar model in mimetic theory. Gen. Relativ. Gravit. **55**, 63 (2023)
14. J. Andrade & D. Santana, An isotropic extension of Einstein's universe solution through gravitational decoupling. Eur. Phys. J. C, **82**(11), 985 (2022)
15. B.C. Nolan and L.V. Nolan, On isotropic cylindrically symmetric stellar models. Class. and Quantum Grav. **21**(15), 3693 (2004)
16. A. Waseem, S. Naeem, Study of isotropic stellar models via Durgapal–Lake solutions in Rastall system. Phys. Scr. **99**, 125023 (2024)
17. L. Herrera, N.O. Santos, Local anisotropy in self-gravitating systems. Phys. Rep. **286**, 53–130 (1997)
18. R. Kippenhahn, A. Weigert, A. Weiss, Stellar Structure and Evolution, Vol. 192 (Springer-Verlag, Berlin, 1990)
19. A.I. Sokolov, Phase transitions in a superfluid neutron liquid. Sov. Phys. JETP **52**, 575 (1980)
20. R.F. Sawyer, Condensed π^- phase in neutron-star matter. Phys. Rev. Lett. **29**, 382 (1972)
21. H. Heiselberg, M. Hjorth-Jensen, Phases of dense matter in neutron stars. Phys. Rep. **328**, 237–327 (2000)
22. J. Binney, S. Tremaine, Galactic Dynamics (Princeton Series in Astrophysics, Princeton, 1987)
23. P.S. Letelier, Anisotropic fluids with two-perfect-fluid components. Phys. Rev. D **22**, 807 (1980)
24. R.P. Pant, S. Gedela, R.K. Bisht, N. Pant, Core-envelope model of super dense star with distinct equation of states. Eur. Phys. J. C **79**, 602 (2019)
25. N. Pant, S. Gedela, R.P. Pant, J. Upreti, R.K. Bisht, Three-layered relativistic stellar model endowed with distinct equation of states. Eur. Phys. J. Plus **135**, 180 (2020)
26. S.S. Yazadjiev, Relativistic models of magnetars: Nonperturbative analytical approach. Phys. Rev. D **85**, 044030 (2012)
27. R. Ciolfi, V. Ferrari, L. Gualtieri, Structure and deformations of strongly magnetized neutron stars with twisted-torus configurations. Mon. Not. R. Astron. Soc. **406**, 2540–2548 (2010)
28. J. Frieben, L. Rezzolla, Equilibrium models of relativistic stars with a toroidal magnetic field. Mon. Not. R. Astron. Soc. **427**, 3406–3426 (2012)
29. V. Canuto, Equation of state at ultrahigh densities. Annu. Rev. Astron. Astrophys. **12**, 167–214 (1974)
30. L. Herrera, A. Di Prisco, J. Hernández-Pastora, N.O. Santos, On the role of density inhomogeneity and local anisotropy in the fate of spherical collapse. Phys. Lett. A **237**, 113–118 (1998)
31. L. Herrera, Stability of the isotropic pressure condition. Phys. Rev. D **101**(10), 104024 (2020)
32. J.H. Jeans, The motions of stars in a Kapteyn universe. Mon. Not. R. Astron. Soc. **82**, 122–132 (1922)
33. G. Lemaître, Ann. Soc. Sci. Brux. A **53**, 51 (1933)
34. R.L. Bowers, E.P.T. Liang, Anisotropic spheres in general relativity. Astrophys. J. **188**, 657 (1974)
35. K. Dev & M. Gleiser, Anisotropic stars: exact solutions. Gen. Relativ. Gravit., **34**(11), 1793–1818(2002)
36. M.K. Mak, T. Harko, An exact anisotropic quark star model. Chin. J. Astron. Astrophys. **2**, 248 (2002)
37. S.K. Maurya & S.D. Maharaj, Anisotropic fluid spheres of embedding class one using Karmarkar condition. Eur. Phys. J. C, **77**(5), 328(2017)
38. M. Malaver, Some new models of anisotropic compact stars with quadratic equation of state. World Sci. News **109**, 180–194 (2018)
39. R.N. Nasheeha, S. Thirukkanesh, F.C. Ragel, Anisotropic models for compact star with various equation of state. Eur. Phys. J. Plus **136**, 132 (2021)
40. M. Kumar, J. Kumar, P. Bharti, A.K. Prasad, Exploring the physics of relativistic compact stars: an anisotropic model with quadratic equation of state in Buchdahl geometry. Astrophys. Space Sci. **369**, 97 (2024)

41. K. Pant, P. Fuloria, A comprehensive analysis of anisotropic stellar objects with quadratic equation of state. Pramana **98**, 158 (2024)
42. S. Das, K.N. Singh, L. Baskey, F. Rahaman, A.K. Aria, Modeling of compact stars: an anisotropic approach. Gen. Relativ. Gravit. **53**, 25 (2021)
43. J. Zdunik, P. Haensel, Maximum mass of neutron stars and strange neutron-star cores. Astron. Astrophys. **551**, A61 (2013)
44. J. M. Lattimer & M. Prakash, The physics of neutron stars. Science, **304**(5670), 536-542(2004)
45. J.M. Lattimer, M. Prakash, The equation of state of hot, dense matter and neutron stars. Phys. Rep. **621**, 127–164 (2016)
46. F. Özel, P. Freire, Masses, radii, and the equation of state of neutron stars. Annu. Rev. Astron. Astrophys. **54**, 401–440 (2016)
47. G. Baym, T. Hatsuda, T. Kojo, P.D. Powell, Y. Song, T. Takatsuka, From hadrons to quarks in neutron stars: a review. Rep. Prog. Phys. **81**, 056902 (2018)
48. C.J. Horowitz, M.A. Perez-Garcia, J. Piekarewicz, Neutrino-"pasta" scattering: The opacity of nonuniform neutron-rich matter. Phys. Rev. C **69**, 045804 (2004)
49. M. Caplan, C. Horowitz, Colloquium: Astromaterial science and nuclear pasta. Rev. Mod. Phys. **89**, 041002 (2017)
50. C. Kouvaris, P. Tinyakov, Can neutron stars constrain dark matter?. Phys. Rev. D **82**, 063531 (2010)
51. J. Bramante, T. Linden, Detecting dark matter with imploding pulsars in the galactic center. Phys. Rev. Lett. **113**(19), 191301 (2014)
52. H. Sotani, K. Kokkotas, N. Stergioulas, Torsional oscillations of relativistic stars with dipole magnetic fields. Mon. Not. R. Astron. Soc. **375**, 261–277 (2007)
53. T. Kuroda, M. Shibata, Failed supernova simulations beyond black hole formation. Mon. Not. R. Astron. Soc. **526**, 152–159 (2023)
54. D. Tsuna, Failed supernova remnants. Publ. Astron. Soc. Jpn. **73**, L6–L11 (2021)
55. C.S. Kochanek, Failed supernovae explain the compact remnant mass function. Astrophys. J. **785**, 28 (2014)
56. C.L. Fryer, P.J. Brown, F. Bufano, J.A. Dahl, C.J. Fontes, L.H. Frey, . . . , P.A. Young, Spectra and light curves of failed supernovae. Astrophys. J. **707**, 193 (2009)
57. J. Neustadt, C. Kochanek, K. Stanek, C. Basinger, T. Jayasinghe, C. Garling, S. Adams, J. Gerke, The search for failed supernovae with the Large Binocular Telescope: a new candidate and the failed SN fraction with 11 yr of data. Mon. Not. R. Astron. Soc. **508**, 516–528 (2021)
58. E. O'Connor, C.D. Ott, Black hole formation in failing core-collapse supernovae. Astrophys. J. **730**, 70 (2011)
59. R. Fernández, E. Quataert, K. Kashiyama, E.R. Coughlin, Mass ejection in failed supernovae: variation with stellar progenitor. Mon. Not. R. Astron. Soc. **476**, 2366–2383 (2018)
60. S.C. Rose, S. Naoz, R.E. Sari, I. Linial, The formation of intermediate-mass black holes in galactic nuclei. Astrophys. J. Lett. **929**, L22 (2022)
61. F.P. Rizzuto, et al., Intermediate mass black hole formation in compact young massive star clusters. Mon. Not. R. Astron. Soc. **501**, 5257–5273 (2021)
62. Y. Sakurai, N. Yoshida, M.S. Fujii, S. Hirano, Formation of intermediate-mass black holes through runaway collisions in the first star clusters. Mon. Not. R. Astron. Soc. **472**, 1677–1684 (2017)
63. M.S. Fujii, L. Wang, A. Tanikawa, Y. Hirai, T.R. Saitoh, Simulations predict intermediate-mass black hole formation in globular clusters. Science **384**, 1488–1492 (2024)
64. J.E. Greene, J. Strader, L.C. Ho, Intermediate-mass black holes. Annu. Rev. Astron. Astrophys. **58**, 257–312 (2020)
65. K. Ruiz-Rocha, et al., Properties of "Lite" Intermediate-mass Black Hole Candidates in LIGO-Virgo's Third Observing Run. Astrophys. J. Lett. **985**, L37 (2025)
66. K. Ruiz-Rocha, K. Holley-Bockelmann, K. Jani, M. Mapelli, S. Dunham, W. Gabella, A Sea of Black Holes: Characterizing the LISA Signature for Stellar-origin Black Hole Binaries. Astrophys. J. **981**, 27 (2025)
67. J. Ovalle, E. Contreras, Z. Stuchlík, Energy exchange between relativistic fluids: the polytropic case. Eur. Phys. J. C **82**, 211 (2022)
68. J. Ovalle, Searching exact solutions for compact stars in braneworld: a conjecture. Mod. Phys. Lett. A **23**, 3247–3263 (2008)
69. J. Ovalle, Decoupling gravitational sources in general relativity: The extended case. Phys. Lett. B, **788**, 213-218(2019)
70. J. Ovalle, Decoupling gravitational sources in general relativity: from perfect to anisotropic fluids. Phys. Rev. D **95**, 104019 (2017)
71. E. Contreras, Z. Stuchlík, Energy exchange between Tolman VII and a polytropic fluid. Eur. Phys. J. C **82**, 365 (2022)
72. S.K. Maurya, M. Govender, G. Mustafa, R. Nag, Relativistic models for vanishing complexity factor and isotropic star in embedding Class I spacetime using extended geometric deformation approach. Eur. Phys. J. C **82**, 1006 (2022)
73. T.T. Smitha, S.K. Maurya, B. Dayanandan, G. Mustafa, Anisotropic star by gravitational decoupling: a vanishing complexity approach. Results Phys. **49**, 106502 (2023)
74. M.A. Habsi, S.K. Maurya, S.A. Badri, M. Al-Alawiya, T.A. Mukhaini, H.A. Malki, G. Mustafa, Self-bound embedding Class I anisotropic stars by gravitational decoupling within vanishing complexity factor formalism. Eur. Phys. J. C **83**, 286 (2023)
75. S.K. Maurya, A. Errehymy, M.K. Jasim, M. Daoud, N. Al-Harbi, A.H. Abdel-Aty, Complexity-free solution generated by gravitational decoupling for anisotropic self-gravitating star in symmetric teleparallel f(Q)-gravity theory. Eur. Phys. J. C **83**, 317 (2023)
76. S.V. Lohakare, S.K. Maurya, K.N. Singh, B. Mishra, A. Errehymy, Influence of three parameters on maximum mass and stability of strange star under linear f(Q)- action. Mon. Not. R. Astron. Soc. **526**, 3796–3814 (2023)
77. S.K. Maurya, K.N. Singh, M. Govender, S. Ray, Complexity-Free Anisotropic Solution of Buchdahl's Model and Energy Exchange Between Relativistic Fluids by Extended Gravitational Decoupling. Fortschr. Phys. **71**, 2300023 (2023)
78. E. Contreras & Z. Stuchlik, A simple protocol to construct solutions with vanishing complexity by Gravitational Decoupling. Eur. Phys. J. C, **82**(8), 706(2022)
79. J. Andrade, D. Santana, Energetic interaction between Einstein's universe and a source like-Tolman IV complexity factor. Int. J. Theor. Phys. **63**, 134 (2024)
80. J. Ovalle, R. Casadio, Beyond Einstein gravity: the minimal geometric deformation approach in the brane-world. Springer Nature, Cham (2020)
81. R. da Rocha, Dark SU(N) glueball stars on fluid branes. Phys. Rev. D **95**, 124017 (2017)
82. A. Fernandes–Silva & R.D. Rocha, Gregory–Laflamme analysis of MGD black strings. Eur. Phys. J. C, **78**(3), 271(2018)

83. R. Casadio, P. Nicolini, R. da Rocha, Generalised uncertainty principle Hawking fermions from minimally geometric deformed black holes. Class. Quantum Grav. **35**, 185001 (2018)
84. A. Fernandes-Silva, A.J. Ferreira-Martins, R. da Rocha, The extended minimal geometric deformation of SU(N) dark glueball condensates. Eur. Phys. J. C **78**, 631 (2018)
85. E. Contreras, P. Bargueño, Minimal geometric deformation decoupling in 2+1 dimensional space–times. Eur. Phys. J. C **78**, 558 (2018)
86. E. Contreras, Minimal Geometric Deformation: the inverse problem. Eur. Phys. J. C, **78**(8), 678(2018)
87. E. Contreras & P. Bargueño, Minimal geometric deformation in asymptotically (A-) dS space-times and the isotropic sector for a polytropic black hole. Eur. Phys. J. C, **78**(12), 985(2018)
88. R. Da Rocha & A.A. Tomaz, Holographic entanglement entropy under the minimal geometric deformation and extensions. Eur. Phys. J. C, **79**(12), 1035(2019)
89. C. Las Heras, P. León, New algorithms to obtain analytical solutions of Einstein's equations in isotropic coordinates. Eur. Phys. J. C **79**, 990 (2019)
90. G. Panotopoulos, Á. Rincón, Minimal geometric deformation in a cloud of strings. Eur. Phys. J. C **78**, 851 (2018)
91. Á. Rincón, L. Gabbanelli, E. Contreras, F. Tello-Ortiz, Minimal geometric deformation in a Reissner–Nordström background. Eur. Phys. J. C **79**, 873 (2019)
92. R. da Rocha, MGD Dirac stars. Symmetry **12**, 508 (2020)
93. E. Contreras, F. Tello-Ortiz, S.K. Maurya, Regular decoupling sector and exterior solutions in the context of MGD. Class. Quantum Grav. **37**, 155002 (2020)
94. C. Arias, F. Tello-Ortiz, E. Contreras, Extra packing of mass of anisotropic interiors induced by MGD. Eur. Phys. J. C **80**, 463 (2020)
95. R. da Rocha, Minimal geometric deformation of Yang-Mills-Dirac stellar configurations. Phys. Rev. D, **102**(2), 024011(2020)
96. R. da Rocha & A.A. Tomaz, MGD-decoupled black holes, anisotropic fluids and holographic entanglement entropy. Eur. Phys. J. C, **80**(9), 857(2020)
97. P. Meert, R. da Rocha, Probing the minimal geometric deformation with trace and Weyl anomalies. Nucl. Phys. B **967**, 115420 (2021)
98. S.K. Maurya, K.N. Singh, M. Govender, S. Hansraj, Gravitationally decoupled strange star model beyond the standard maximum mass limit in Einstein–Gauss–Bonnet gravity. Astrophys. J. **925**, 208 (2022)
99. S.S. Medina, J. Andrade, D. Santana, T. Naseer, Effect of gravitational cracking on energy exchange in relativistic fluids: a first approach. Eur. Phys. J. C **85**, 1–13 (2025)
100. M. Wyman, Schwarzschild interior solution in an isotropic coordinate system. Phys. Rev. **70**, 74 (1946)
101. J. Andrade & E. Contreras, Stellar models with like-Tolman IV complexity factor. Eur. Phys. J. C, **81**(10), 889(2021)
102. J. Andrade, D. Andrade, Stellar models with like-Wyman IIa complexity factor. J. Phys.: Conf. Ser. **2796**, 012007 (2024)
103. D. Santana, E. Fuenmayor, E. Contreras, Integration of the Lane–Emden equation for relativistic anisotropic polytropes through gravitational decoupling: a novel approach. Eur. Phys. J. C **82**, 703 (2022)
104. G. Abellán, E. Fuenmayor, L. Herrera, The double polytrope for anisotropic matter: Newtonian case. Phys. Dark Univ. **28**, 100549 (2020)
105. L. Herrera & W. Barreto, Newtonian polytropes for anisotropic matter: General framework and applications. Phys. Rev. D, **87**(8), 087303(2013)
106. G.P. Horedt, Polytropes: applications in astrophysics and related fields. Springer, Dordrecht (2004)
107. B.V. Ivanov, Analytical study of anisotropic compact star models. Eur. Phys. J. C, **77**(11), 738(2017)
108. B.V. Ivanov, Maximum bounds on the surface redshift of anisotropic stars. Phys. Rev. D **65**, 104011 (2002)
109. H.A. Buchdahl, General relativistic fluid spheres. Phys. Rev. **116**, 1027 (1959)
110. W. Gander, W. Gautschi, Adaptive quadrature-revisited. BIT Numer. Math. **40**, 84–101 (2000)
111. M. Visser, C. Barcelo, Energy conditions and their cosmological implications. In: 3rd Int. Conf. on Particle Phys. and the Early Universe, pp. 98–112 (2000, September)

Eur. Phys. J. C manuscript No.
(will be inserted by the editor)

Energy exchange between a relativistic polytrope and a Wyman IIa fluid

Jorge Gallegos [1], **Domnica Quizhpe**[1], **J. Andrade**[a,1], **Marlon Moscoso-Martnez**[b,1,2], **Tayyab Naseer** [c,3,4]

[1]Escuela Superior Politcnica de Chimborazo, (ESPOCH), Riobamba 060155, Ecuador
[2]Higher School of Engineering and Technology, Universidad Internacional de la Rioja (UNIR), Avda. de la Paz 137, Logroño, 26006, España
[3]Department of Mathematics and Statistics, The University of Lahore, 1-KM Defence Road, Lahore 54000, Pakistan
[4]Research Center of Astrophysics and Cosmology, Khazar University, Baku, AZ1096, 41 Mehseti Street, Azerbaijan

Received: date / Accepted: date

Abstract A detailed analysis of the energy exchange between a relativistic polytrope and an isotropic Wyman IIa fluid within a compact stellar object is presented. This investigation uses the theoretical framework of gravitational decoupling by extended minimal geometric deformation as its central axis. The results show that the polytrope transfers energy to the Wyman IIa fluid in the outer layers of the system, while the core remains stable without any energy transfer. Furthermore, it is verified that the effective compact system is physically realistic for configurations satisfying the well-known strong energy condition for anisotropic self-gravitating spheres, since its violation in this case leads to unstable configurations.

1 Introduction

One of the best natural laboratories for exploring the limits of physical knowledge is stellar remnants. Such astrophysical configurations are notable for their extreme conditions, such as high density, strong magnetic fields, high temperatures, and so on. Specifically, their high density leads to the generation of high gravitational fields, which can even tear the fabric of spacetime apart in the extreme case of black holes. This is why the use of the modern theory of general relativity is essential to unravel their mysteries, given that the use of Newtonian gravitation is no longer reliable in these extreme regimes. The theoretical study of these fascinating objects began with the discovery of the first solution to Einstein's Field Equations (EFE) [1, 2] by K. Schwarzschild, both as an internal and external solution of an isotropic, homogeneous, self-gravitating sphere [3, 4]. Later, solutions in the isotropic pressure regime were found; for example, works such as [5–16]. Such solutions, however, do not fully describe more realistic stellar systems since they present local deviation from isotropy due to various aspects that are very specific to these astrophysical objects, such as their high density, strong magnetic fields, rotation, high temperature, internal phase transitions, presence of solid cores, etc [17–30]. Indeed, this aspect has been demonstrated to be a result of the stellar evolution of these objects [31], and therefore results in a physical interest in the construction of this kind of model in the regimen of anisotropic pressure.

The first hint of the real possibility of the presence of anisotropy in stellar fluids due to stellar velocity dispersion was developed by Jean in [32]. Indeed, Einstein noticed that the spherical symmetry in EFE maintains equality only in the two tangential pressures, and subsequently this was indicated also by Lemaitre in 1933 [33]. This fact has been reinforced by Ruderman, who showed theoretically that in very high-density regimes typical of stellar remnants larger than $10^{15}\ g/cm^3$, the anisotropy in pressures seems to be a natural aspect. Subsequently, Bowers and Liang examined this aspect in [34]. They found that anisotropy plays a very important role in the stability of stellar remnants and that it is more likely to occur in the outer parts of compact stars than in the core. Subsequently, many studies have been carried out multiple subsequent studies that take into account the anisotropy in the interior of these fascinating astrophysical objects, such as [35–42].

[a]e-mail: julio.andrade@espoch.edu.ec
[b]e-mail: marlon.moscoso@espoch.edu.ec;marlonernesto.moscoso-externo@unir.net
[c]e-mail: tayyabnaseer48@yahoo.com;tayyab.naseer@khazar.org;tayyab.naseer@math.uol.edu.pk

Despite the extensive previous work carried out in this area of stellar remnants, there are still open physical aspects to be clarified regarding these natural laboratories. For example, we do not fully understand the behavior of matter at densities higher than the atomic nucleus (in the core of a neutron star, for example [43–52]), such as the process that gives rise to the formation of intermediate-mass black holes, such as the process of black hole birth without the appearance of supernovae, among others [53–66]. In particular, the dynamics of the fluids within these compact objects is of great interest. It should be noted that the detailed determination of the coexistence of relativistic fluids inside stellar remnants can be very complex in itself, for many reasons, such as the variability of their nature, the complex ways in which they interact, and, above all, their behaviour under the extreme physical conditions to which they are confined. An intriguing aspect related to such coexistence is the energy interaction between the fluid components inside a stellar compact object, a point that was investigated in [67], where the energy exchange between a polytropic fluid and a generic isotropic fluid was developed based on the use of gravitational decoupling (GD) by extended geometric deformation (MGDe) [68–70]. This approach is highlighted since it permits the study of the energy exchange of the fluid components without resolving the Lane-Emden equation, which does not have analytic solutions. It is possible since this framework solves the problem of EFE for a tensor momentum that is a combination of several sources, that is, $T_{\mu\nu} = T^1_{\mu\nu} + T^2_{\mu\nu} + \cdots + T^n_{\mu\nu}$ in an analytical way. Even the role of each source $T^i_{\mu\nu}$ can be explored, and therefore it is possible to study the total exchange energy between the interior components.

In [67] the well-known Tolman IV solution is considered interacting with a relativistic polytrope where the maximum interaction is presented in the stellar surface with a positive gradient of energy in the radial direction. Subsequently, the energy exchange between the Tolman VII perfect fluid and a polytrope fluid was investigated. In this case such energy exchange is minimum at the centre, having a maximum value at some inner core located around it, and then decreases again towards the surface in contrast to [71]. In both cases, the polytrope fluid releases energy to the environment in order to sustain the static self-gravitating sphere. Thus the framework of GD by MGDe later inspired works such as this, as various aspects of this energy exchange have been studied [72–79]. These studies are vitally important in determining which fluids are most dominant in internal energy exchange and which areas have the most outstanding energy dynamics. It can give us important clues related to the main processes of its evolution and stellar stability. Also, we have to mention that the GD has been widely used in the construction of physically viable models of stellar compact objects [80–98]. This method has even been used recently as a basis for understanding the great influence of the appearance of internal fractures that appear when a compact star system leaves its stellar equilibrium, influencing the energy exchange between relativistic fluids within a compact object (see details in Ref. [99]).

This work seeks to contribute to the understanding of the dynamics of energy exchange within stellar compact objects, specifically in the case of a polytrope with an isotropic fluid type Wyman IIa. For this study, we use the GD by MGDe, taking into account a mimic constraint for the energy density in order to close the generated mathematical problem. The application of the aforementioned method resulted in the use of a numerical approach given the high complexity of the isotropic fluid metric used. Our findings show us that the politrope fluid component plays a fundamental role in the dynamics of energy exchange inside the stellar object. This study is particularly important because it will rigorously analyse the conditions of physical acceptability despite the complexity of the fluid metric.

The present manuscript is organised as follows: In Section 2 we explain the methodology based on gravitational decoupling (GD) by extended minimum geometric deformation (MGDe) to analyse the energy exchange between different gravitational sources; in Section 3 we present the physical acceptability conditions; in Section 4 we describe the analytical development for obtaining the new solution; in Section 5 we present the physical acceptability analysis for this new model; finally, in Section 6 we present conclusions, where we discuss implications and future perspectives.

2 Gravitational decoupling by extended minimal geometric deformation

In this section, we shall briefly review the theoretical framework of GD by MGDe [68–70]. The GD solves the problem of EFE

$$G_{\mu\nu} \equiv R_{\mu\nu} - \frac{1}{2} R g_{\mu\nu} = \kappa T_{\mu\nu}. \tag{1}$$

with

$$T_{\mu\nu} = T^{(s)}_{\mu\nu} + \Theta_{\mu\nu}, \tag{2}$$

where $T^{(s)}_{\mu\nu}$ is known gravitational source, $\Theta_{\mu\nu}$ is an unknown source, and $\kappa = \frac{8\pi G}{c^4}$. At this stage, it is pertinent to elucidate the motivation behind employing the GD approach via MGDe in this study. The

GD framework offers a powerful and systematic method to address the complexity of solving EFE for systems with multiple interacting matter sources, such as the relativistic polytrope and Wyman IIa fluid considered here. By decomposing the total energy-momentum tensor into a known seed source and an additional source , the GD approach allows for the analytical separation of the field equations into manageable subsystems. This decoupling is particularly advantageous in modeling compact stellar objects, where the interplay between different fluid components under extreme gravitational conditions introduces significant mathematical challenges. The MGDe technique enhances this framework by introducing MGD to the metric components, as described in subsequent sections. This method preserves the spherical symmetry of the system while enabling the exploration of anisotropic effects arising from the interaction between the seed and additional sources. Such an approach is crucial for studying energy exchange dynamics, as it provides a tractable pathway to analyze the physical implications of each sources contribution without requiring the direct solution of highly nonlinear equations, such as the Lane-Emden equation for polytropes. Furthermore, the GD approach facilitates the investigation of physically realistic configurations by allowing the imposition of constraints, such as the mimic constraint for energy density used in this work, to close the system of equations. This flexibility makes GD via MGDe an ideal tool for probing the intricate physics of compact stars, offering insights into their stability, structure, and evolutionary processes that are otherwise difficult to obtain through traditional methods.

The effective solution of this problem is a static sphere self-gravitating whose interior space-time is given by

$$ds^2 = e^{\nu}dt^2 - e^{\lambda}dr^2 - r^2 d\Omega^2, \tag{3}$$

where $d\Omega^2 = d\theta^2 + \sin^2\theta d\phi^2$, $\nu(r)$ and $\lambda(r)$ are functions of the radial coordinate r. Thus, we can use this fact, namely, if we use the metric (3) in EFE (1), the effective matter sector of this static sphere is found as:

$$\kappa\rho = \frac{1}{r^2} - e^{-\lambda}\left(\frac{1}{r^2} - \frac{\lambda'}{r}\right), \tag{4}$$

$$\kappa p_r = \frac{1}{r^2} - e^{-\lambda}\left(\frac{1}{r^2} + \frac{\nu'}{r}\right), \tag{5}$$

$$\kappa p_t = -\frac{e^{-\lambda}}{4}\left(2\nu'' + \nu'^2 - \lambda'\nu' + 2\frac{\nu' - \lambda'}{r}\right). \tag{6}$$

These physical quantities are given by:

$$\rho = T_0^{0(s)} + \Theta_0^0, \tag{7}$$

$$p_r = -T_1^{1(s)} - \Theta_1^1, \tag{8}$$

$$p_t = -T_2^{2(s)} - \Theta_2^2, \tag{9}$$

which is the matter sector of an anisotropic fluid static sphere.

Now, it is pertinent to emphasize that GD via MGDe is based in the idea that the seed source $T_{\mu\nu}^{(s)}$ whose space-time:

$$ds^2 = e^{\xi(r)}dt^2 - e^{\mu(r)}dr^2 - r^2 d\Omega^2, \tag{10}$$

is influenced by the extra unknown source $\theta_{\mu\nu}$ in such way its space-time is deformed as:

$$\xi \to v = \xi + g, \tag{11}$$

$$e^{-\mu} \to e^{-\lambda} = e^{-\mu} + f, \tag{12}$$

where f and g are functions only of the radial coordinate, and are known as geometric deformations. It should be noted that these functions must only have dependence on r to maintain the perfect spherical symmetry of the final solution. After, it is crucial to inserts the equations (11)-(12) into (4)-(6), it yields two systems of differential equations:
The first set related to the seed source $T_{\mu\nu}^{(s)}$:

$$\kappa T_0^{0(s)} = \frac{1}{r^2} - e^{-\mu}\left(\frac{1}{r^2} - \frac{\mu'}{r}\right), \tag{13}$$

$$\kappa T_1^{1(s)} = -\frac{1}{r^2} + e^{-\mu}\left(\frac{1}{r^2} + \frac{\xi'}{r}\right), \tag{14}$$

$$\kappa T_2^{2(s)} = \frac{e^{-\mu}}{4}\left(2\xi'' + \xi'^2 - \mu'\xi' + 2\frac{\xi' - \mu'}{r}\right), \tag{15}$$

and the second source-related set $\Theta_{\mu\nu}$:

$$\kappa\Theta_0^0 = -\frac{f}{r^2} - \frac{f'}{r}, \tag{16}$$

$$\kappa\Theta_1^1 - \mathcal{J}_1 = f\left(\frac{1}{r^2} + \frac{\nu'}{r}\right), \tag{17}$$

$$\kappa\Theta_2^2 - \mathcal{J}_2 = \frac{f}{4}\left(2\nu'' + \nu'^2 + 2\frac{\nu'}{r}\right) - \frac{f'}{4}\left(\nu' + \frac{2}{r}\right), \tag{18}$$

where $\mathcal{J}_1 = \frac{e^{-\mu}g'}{r}$ and $4\mathcal{J}_2 = e^{-\mu}\left(2g'' + g'^2 + \frac{2g'}{r} + 2\xi'g' - '\,\mu'g'\right)$.

Precisely the possibility of decoupling the initial problem in these two systems of equations is the key to the success of GD and is what gives this method its name.

Also, it is important to mention that since the Bianchi identities are satisfied by $G_{\mu\nu}$ then

$$\nabla_\mu T^{\mu\nu} = 0, \tag{19}$$

also is satisfied. Thus, using the energy-momentum tensor (2) into (19), we obtain (see the calculation details in [67]):

$$\nabla_\sigma T^{\sigma(s)}_\nu = -\nabla_\sigma \Theta^\sigma_\nu = -\frac{g'}{2}\left(T^{0(s)}_0 - T^{1(s)}_1\right)\delta^\sigma_\nu. \tag{20}$$

The above equation has a prominent importance given that it determines the energy interchange between the relativistic fluids $\{T^{(s)}_{\mu\nu}, \Theta_{\mu,\nu}\}$ that sustain the self-gravitating sphere; indeed, it gives us:

$$\Delta E = \frac{g'}{2\kappa}\frac{e^{-\mu}}{r}(\xi' + \mu'), \tag{21}$$

where, if $g' > 0$ implies that $\Delta E > 0$, that is, the source $\Theta_{\mu\nu}$ releases energy to the environment, while if $g' < 0$, then $T^{(s)}_{\mu\nu}$ is the one that provides its energy so that the two fluids can coexist within the self-gravitating sphere. This result is too important, since it permits modeling the energy interaction between the fluids that support a self-gravitating sphere.

Specifically, the above development is a precursor to the possibility of studying the energy exchange between relativistic fluids that form a compact stellar object. These studies have already been mentioned above. Thus, our objective is to use this method, together with the one developed in [67], to study the possibility of having realistic compact stellar configurations supported by two stellar fluids, such as the isotropic Wyman IIa fluid ($n = 1$) and a relativistic polytropic fluid, and to examine the dynamics of the energy exchange between them.

But before constructing this effective model, let's review a little about the relativistic fluids that support it, as well as the conditions of physical acceptability that our effective model must meet.

2.1 Wyman IIa isotropic fluid

For this research we used as a known source $T^{(s)}_{\mu\nu}$ the Wyman IIa solution (with $n = 1$), which is an isotropic stellar fluid whose metric is [7,100]:

$$e^{\xi} = (A - Br^2)^2, \tag{22}$$

$$e^{-\mu} = 1 + Cr^2(A - 3Br^2)^{-\frac{2}{3}}, \tag{23}$$

where A is a dimensionless constant, while B and C are constants with dimensions inverse to the length squared. The selection of such a fluid as the seed source in this study is driven by its well-established physical properties and its applicability within the framework of general relativity for modeling compact stellar objects. The Wyman IIa solution, characterized by its isotropic pressure profile and analytical tractability, provides a robust foundation for studying complex relativistic systems. Its metric offers a mathematically consistent and physically realistic description of a self-gravitating sphere, making it an ideal candidate for exploring energy interactions with a relativistic polytrope. Furthermore, the Wyman IIa fluids prior successful application in gravitational decoupling studies, underscores its versatility in generating new stellar models. By choosing this fluid, we ensure a reliable starting point that facilitates the analytical and numerical exploration of energy exchange dynamics while maintaining compatibility with the physical acceptability conditions required for realistic compact star configurations. This choice also allows for a direct comparison with previous studies involving other isotropic fluids, such as Tolman IV and Tolman VII, thereby contributing to a broader understanding of fluid interactions in stellar remnants.

The matter sector of this interior solution is

$$T^{0(s)}_0 = \rho^{(s)} = \frac{(5Br^2 - 3A)\,C}{\kappa\,(A - 3Br^2)^{5/3}}, \tag{24}$$

$$T^{1(s)}_1 = T^{2(s)}_2 = T^{3(s)}_3 = p^{(s)} = \frac{\left(5 - \frac{4A}{A - Br^2}\right)\left(\frac{Cr^2}{(A - 3Br^2)^{2/3}} + 1\right) - 1}{\kappa r^2} \tag{25}$$

This solution has previously been used as a seed solution within the GD method for the purpose of finding new stellar models in [101–103]. This is why we chose this seed, which does not preclude working with other seed solutions in future works.

2.2 Polytrope

Now, the unknown source $\Theta_{\mu\nu}$ is considered as a relativistic polytrope whose equation of state can be written as

$$P_r = K\rho^{\Gamma}_\Theta = K\rho^{1+\frac{1}{n}}_\Theta, \tag{26}$$

where P_r is the isotropic pressure and ρ_Θ is the (baryonic) mass density. The constants K, Γ, and n are usually referred to as the polytropic constant, polytropic exponent, and polytropic index, respectively. From the above, we know that this equation of state will only depend on the pressure, $\rho_\Theta = \rho_\Theta(P_r)$ [18]. When the constant K is calculated from natural constants, the polytropic equation of state can be used to model a non-relativistic, completely degenerate Fermi gas ($n = 5/3$), and in the relativistic limit ($n = 4/3$). Otherwise, if K is a free parameter, the models can be used to describe an isothermal ideal gas or a completely convective star. Polytropes are also known to play an important role in

the study of stellar structures for several fundamental astrophysical problems. For example, objects such as anisotropic white dwarfs have been modelled considering a general formalism to study Newtonian polytropes for anisotropic matter [**?**, 104, 105].

Furthermore, this choice is particularly advantageous in the context of MGDe, as it simplifies the analytical treatment of the energy-momentum tensor for the additional source. The polytropic model facilitates the exploration of energy exchange dynamics between the relativistic polytrope and the isotropic Wyman IIa fluid, enabling a tractable analysis of their interaction without the need to solve the complex Lane-Emden equation numerically. Furthermore, the polytropic equation of state is well-suited for studying the stability and structural properties of compact objects, as it accounts for the effects of high-density environments and anisotropic pressures, which are critical for understanding the physical realism of the resulting stellar configurations. This approach aligns with established astrophysical models and provides a robust foundation for investigating the intricate interplay of relativistic fluids within self-gravitating systems. Note that that we have used the subscript Θ in Eq. (26) to avoid confusion with the total density of the effective system in our work.

3 Physical acceptability conditions

Every anisotropic interior solution must meet a set of physical acceptability conditions in order to model a realistic compact star. These are detailed in [107]:

1. **Regular space - time**
   The spacetime metric components of the interior solution are positive functions; they must be finite and free of singularities inside the star. At the centre, they must satisfy $e^{-\lambda(0)} = 1$ and $e^{\nu(0)} = constant$. Furthermore, $e^{-\lambda}$ is a monotonically decreasing function and e^{ν} is monotonically increasing.
2. **Matching conditions**
   On the surface of the star $r = R$ the interior solution must coincide with the exterior Schwarzschild solution, which determines that:
   $$e^{\nu(r=R)} = e^{-\lambda(r=R)} = 1 - \frac{2M}{R}, \tag{27}$$
   where R is the radius of the star and M its total mass.
   Likewise, the radial pressure at this point disappears
   $$p_r(r = R) = 0, \tag{28}$$
   because there is emptiness outside the compact star.
3. **Causality condition**
   The radial velocity $v_r^2 = \frac{dp_r}{d\rho}$ and tangential velocity $v_t^2 = \frac{dp_t}{d\rho}$ of sound inside the stellar object must not exceed the causal limit of the speed of light ($c = 1$); therefore:
   $$0 \leq v_r^2 < 1 \quad \text{and} \quad 0 \leq v_t^2 < 1. \tag{29}$$
4. **Matter sector**
   The quantities ρ, p_r, p_t must be positive, monotonically decreasing, and continuous functions. Furthermore, they reach their maximum at the centre, that is, $\rho'(0) = p_r'(0) = p_t'(0) = 0$. The tangential pressure must remain greater than the radial pressure inside the star, with the exception of the centre, where $p_t(0) = p_r(0)$.
5. **Energy conditions**
   The material sector of the solution must satisfy the dominant energy condition (DEC):
   $$\rho \geq p_r, \quad \text{and} \quad \rho \geq p_t. \tag{30}$$
   It is desirable but not mandatory that the strong energy condition (SEC):
   $$\rho \geq p_r + 2p_t, \tag{31}$$
   be fulfilled.
6. **Redshift**
   The redshift function $Z(r) = \frac{1}{\sqrt{e^{\nu}}} - 1$ must be continuous and positive, decreasing with the radial variable r. Its value on the surface $Z(r = R)$ has to be less than the universal limit $Z_{\text{bound}} = 5.211$. And if the solution satisfies the SEC, then the limit is $Z_{\text{bound}} = 3.842$ [108, 109].

Now with all this shown above, we show below the construction of our effective compact stellar model.

4 Effective stellar model

First of all, to build our effective interior solution, we will remember that the resulting self-gravitating sphere is composed of two relativistic fluids: one, the seed source $T_{\mu\nu}$ given by

$$T_{\nu}^{\mu(s)} = diag[\rho^{(s)}, -p_r^{(s)}, -p_t^{(s)}, -p_t^{(s)}], \tag{32}$$

which we consider the Wyman IIa fluid; and the other source $\Theta_{\mu\nu}$ is given an isotropic politrope whose matter sector is given by

$$\theta_{\nu}^{\mu} = diag[\rho_{\Theta}, -P_r, -P_r, -P_r]. \tag{33}$$

After, we will use the mimic constraint for the energy density

$$\rho_{\Theta} \sim \rho^{(s)}, \tag{34}$$

in order to study the energy interaction between these fluids with the help of the GD by MGDe approach.

In fact, we use the method developed in [67], where two ways are proposed: one is the aforementioned mimic constraint for energy density and the other is the mimic constraint for pressure. We check both ways for our case, and the way described by the mimic pressure constraint results in a non-viable result because of the difficulties in calculations.

Now, the most simple expression that satisfies (34) is:

$$\rho_{\Theta}(r) = \alpha(K,\Gamma)\rho^{(s)}, \tag{35}$$

where we use a new quantity $\alpha(K,\Gamma)$, which is consistent with the polytrope equation, (26), and with the condition $f(r)|_{K=0} = 0$, which is expressed as follows:

$$\alpha(K,\Gamma) = K^{\Gamma}. \tag{36}$$

Precisely, using the Eq. (35) in EFE (13)-(18), the following differential equation emerges:

$$\frac{f'(r)}{r} + \frac{f(r)}{r^2} = -K^{\Gamma}\left[\frac{1}{r^2} - e^{-\mu(r)}\left(\frac{1}{r^2} - \frac{\mu'(r)}{r}\right)\right] \tag{37}$$

This above differential equation is resolved using the metric component (23), which yields

$$f = \frac{CK^{1+\frac{1}{n}}\, r^2}{(A - 3Br^2)^{\frac{2}{3}}}. \tag{38}$$

Thus, the deformation function f has been found; the next step is to find the function g. To do this, we calculate first $g'(r)$ through the polytrope equation (26) and Eq. (35), giving us:

$$P_r = K(K^{\Gamma}\rho^{(s)})^{\Gamma}. \tag{39}$$

Then using the EFE (13)-(18), which results in

$$g' = \frac{r}{e^{-\mu} + f}\left[\kappa K\left(\frac{(K)^{\Gamma}}{\kappa}\left(\frac{1}{r^2} - e^{-\mu}\left(\frac{1}{r^2} - \frac{\mu'}{r}\right)\right)\right)^{\Gamma} - f\left(\frac{1}{r^2} + \frac{\xi'}{r}\right)\right]. \tag{40}$$

This previous expression is easy to find explicitly with the help of the equations (23) and (38), thus we have:

$$g' = \frac{r}{1 + \frac{C\left(1+K^{1+\frac{1}{n}}\right)r^2}{(A-3Br^2)^{\frac{2}{3}}}}\left[-\frac{CK^{1+\frac{1}{n}}(A - 5Br^2)}{(A - 3Br^2)^{\frac{2}{3}}(A - Br^2)} + K\left(-\frac{CK^{1+\frac{1}{n}}(3A - 5Br^2)}{(A - 3Br^2)^{\frac{5}{3}}\kappa}\right)^{1+\frac{1}{n}}\kappa\right] \tag{41}$$

At this point it is worth emphasising that it is true that with only the information of g' one can find the effective material sector given by the field equations (4)-(6), since they depend only on ν' and not on ν (see equations (11)-(12)); but in this work we want to go a step further than previous works in which the effective material sector is studied, but the effective space-time is neglected, which seems very important to us when ensuring the plausibility of our model in its entirety. Thus, if we are going to calculate g, even if it is numerically given the difficulty of integrating the expression of g'.

To obtain g, we use the variable change of $r \to xR$ to work in units of star radius, so we consider an integration interval of $[0,1]$. Therefore, the g function can be written as

$$g = \int_0^1 \left[\frac{R^2 x}{1 + \frac{C\left(1+K^{1+\frac{1}{n}}\right)R^2x^2}{(A-3BR^2x^2)^{\frac{2}{3}}}}\right] \times \left[-\frac{CK^{1+\frac{1}{n}}(A - 5BR^2x^2)}{(A - 3BR^2x^2)^{\frac{2}{3}}(A - BR^2x^2)} + K\left(-\frac{CK^{1+\frac{1}{n}}(3A - 5BR^2x^2)}{(A - 3BR^2x^2)^{\frac{5}{3}}\kappa}\right)^{1+\frac{1}{n}}\kappa\right]\mathrm{d}x. \tag{42}$$

To evaluate the integral involved in the model, once values were assigned to the free parameters $[A, B, C, K, R, n, \kappa]$, we employed the *global adaptive quadrature method* proposed by Gander and Gautschi [110]. This algorithm is particularly suitable for integrands that present peaks, steep gradients, or complicated behaviour within the integration interval.

The method is based on the systematic subdivision of the integration domain into smaller subintervals, where high-order quadrature rules are applied. The algorithm adaptively refines those subintervals in which the local error estimate exceeds a prescribed tolerance, thereby ensuring an efficient allocation of evaluation points. Unlike local refinement strategies, the global adaptive approach provides control of the error across the entire interval, which guarantees both robustness and accuracy.

This strategy is especially advantageous in relativistic stellar models, where the integrands often display singular-like features or rapid variations near the stellar surface. By applying the GanderGautschi algorithm, it is possible to obtain a reliable and precise evaluation of the integrals without requiring an a priori regularization of the integrand, making it a natural choice for this class of problems.

4.1 Effective space-time

Now, let's find the physical quantities that represent our model. Thus, in order to obtain the effective space-time, we use the Eq. (37) and (23) in (12) resulting in:

$$e^{\lambda}=1+\frac{C(1+K^{1+1/n})r^2}{(A-3Br^2)^{2/3}}. \tag{43}$$

Respect for the temporal metric component is found using Eq. (41) in Eq. (23), and taking into account the fact that $\nu'=\xi'+g'$, we obtain

$$\begin{aligned}\nu'=&-\frac{4Br}{A-Br^2}+\frac{r}{1+\frac{C(1+K^{1+\frac{1}{n}})r^2}{(A-3Br^2)^{\frac{2}{3}}}}\times\\&\left[-\frac{C\,K^{1+\frac{1}{n}}(A-5Br^2)}{(A-3Br^2)^{\frac{2}{3}}(A-Br^2)}\right.\\&\left.+K\left(-\frac{C\,K^{1+\frac{1}{n}}(3A-5Br^2)}{(A-3Br^2)^{\frac{5}{3}}\kappa}\right)^{1+\frac{1}{n}}\kappa\right].\end{aligned} \tag{44}$$

Now as we found the value of g numerically, then the value of ν is found as

$$\nu=\xi+g=\ln(A-Br^2)^2+g, \tag{45}$$

namely

$$e^{\nu}=c_1\left(A-BR^2\right)^2, \tag{46}$$

where c_1 represents a constant that varies according to the numerical value of the integral given by Eq. (42).

4.2 New matter sector

As for the effective material sector, this is found by using (43) and (44) into the EFE (4)-(6). Hence, we find:

$$\rho=-\frac{C\left(K^{\frac{1}{n}+1}+1\right)(3A-5Br^2)}{\kappa\,(A-3Br^2)^{5/3}}, \tag{47}$$

$$\begin{aligned}p_r=&\frac{\kappa\,K\,(A-Br^2)(A-3Br^2)}{\kappa(A-3Br^2)(A-Br^2)}\times\\&\left(-\frac{CK^{\frac{1}{n}+1}(3A-5Br^2)}{\kappa(A-3Br^2)^{5/3}}\right)^{\frac{1}{n}+1}\\&+\frac{C(A-5Br^2)\sqrt[3]{A-3Br^2}}{\kappa(A-3Br^2)(A-Br^2)}\\&+\frac{-4AB+12B^2r^2}{\kappa(A-3Br^2)(A-Br^2)}.\end{aligned} \tag{48}$$

$$\begin{aligned}p_t=&\frac{1}{4\,(A-3Br^2)^{8/3}}\left[\frac{20BCr^2\left(A-3Br^2\right)^2}{A-Br^2}\times\right.\\&K^{1+\frac{1}{n}}\\&+\frac{4BCr^2\left(A-3Br^2\right)^2(A-5Br^2)\,K^{1+\frac{1}{n}}}{(A-Br^2)^2}\\&-\frac{4C\,(A-5Br^2)\left(A-3Br^2\right)^2K^{1+\frac{1}{n}}}{A-Br^2}\\&-\frac{8BCr^2\,(A-5Br^2)\left(A-3Br^2\right)K^{1+\frac{1}{n}}}{A-Br^2}\\&+\frac{2C^2\left(K^{1+\frac{1}{n}}+1\right)r^2\left(A-3Br^2\right)}{(A-3Br^2)^{2/3}+C\left(K^{1+\frac{1}{n}}+1\right)r^2}\times\\&(A-5Br^2)\,K^{1+\frac{1}{n}}\\&+\frac{C^2r^2\left(A-3Br^2\right)^2(A-5Br^2)^2K^{2+\frac{2}{n}}}{(A-Br^2)^2}\\&\left((A-3Br^2)^{2/3}+C\left(K^{1+\frac{1}{n}}+1\right)r^2\right)^{-1}\\&+\frac{C^2r^2\left(3A-5Br^2\right)^2}{(A-3Br^2)^{2/3}+C\left(K^{1+\frac{1}{n}}+1\right)r^2}\times\\&\left(-\frac{CK^{1+\frac{1}{n}}\left(3A-5Br^2\right)}{(A-3Br^2)^{5/3}\,\kappa}\right)^{2/n}K^{4+\frac{2}{n}}\\&-8BC\left(K^{1+\frac{1}{n}}+1\right)r^2\left(A-3Br^2\right)\\&+4C\left(K^{1+\frac{1}{n}}+1\right)(A-Br^2)\left(A-3Br^2\right)\\&-\frac{16B\left(A-3Br^2\right)^2}{A-Br^2}\times\\&\left((A-3Br^2)^{2/3}+C\left(K^{1+\frac{1}{n}}+1\right)r^2\right)\\&-\frac{2CK^{2+\frac{1}{n}}}{n\,(A-Br^2)}\times\\&\left((A-3Br^2)^{2/3}+C\left(K^{1+\frac{1}{n}}+1\right)r^2\right)^{-1}\\&\left.\chi(r)\left(-\frac{CK^{1+\frac{1}{n}}\left(3A-5Br^2\right)}{(A-3Br^2)^{5/3}\,\kappa}\right)^{1/n}\right],\end{aligned} \tag{49}$$

with

$$\begin{aligned}\chi=&\,5B^3\Big(2(2-7n)\left(A-3Br^2\right)^{2/3}\\&+C\left(2(n+2)K^{1+\frac{1}{n}}-13n+4\right)r^2\Big)r^6\\&+AB^2\Big(2(37n-20)\left(A-3Br^2\right)^{2/3}\\&+C\left(-8(3n+5)K^{1+\frac{1}{n}}+61n-40\right)r^2\Big)r^4\\&+A^2B\Big(2(10-13n)\left(A-3Br^2\right)^{2/3}\end{aligned}$$

$$+C\left(2(7n+10)K^{1+\frac{1}{n}}-15n+20\right)r^2\Bigg)r^2$$
$$+3A^3n\left(2\left(A-3Br^2\right)^{2/3}+Cr^2\right) \quad (50)$$

Using the matching conditions (27) with (43) and (46), we then obtain the following relations:

$$A=BR^2+\sqrt{\frac{R-2M}{c_1R}}, \quad (51)$$

$$C=-\frac{2M\left(A-3BR^2\right)^{2/3}}{R^3\left(\mathrm{K}^{\frac{1}{n}+1}+1\right)}. \quad (52)$$

where the constant c_1 depends on the integration of Eq. (42).

On the other hand, if we try to apply the condition (28) in p_r given by Eq. (48) analytically becomes complex issue. This difficulty was raised through a numerical treatment that focuses on obtaining a compactness factor $u=\frac{M}{R}$ such that this condition is met. To do this, in the equation (48), we use the change of variables $M\to uR, r\to xR$, which results in an equation that no longer depends on r. In this way, by evaluating R and x as one (in units of the stellar radius), we managed to obtain an equation that can be solved for u. This procedure was necessary to obtain realistic behaviour of our model.

5 Results

In this part, we analyze first the physical acceptability of the stellar model and then the energy exchange between the fluids that compose the self-gravitating sphere that represents such a model. We checked that the model behaves well with $B=0.45$ with the restriction (52) and the restriction given by Eq. (51), where the parameter c_1 is determined by Eq. (42), and also behaves very regularly for the polytropic index of $n=0.5$. Therefore, our model is precisely the interior of a stellar compact object that is supported by an isotropic fluid type Wyman IIa ($n=1$) and a politrope that is typical in the interior of a neutron star [**?**]. Thus, we have a compact object with a very exotic interior.

We reviewed that finding configurations that satisfy all the conditions of physical acceptability was not an easy task; in fact, small variations in the parameters give physically unrealistic results. In this sense, we have focused on the following configurations for the physical analysis of the model: $K=0.43$ with $u=0.302917$, which is shown in all figures below in the black line, $K=0.44$ with $u=0.334079$ (in the blue line) and $K=0.47$ with $u=0.176426$ (in the red line).

5.1 Acceptability physical analysis

5.1.1 Matter sector

We first plot the profile of the matter sector $\{\rho, p_r, p_t\}$ in Figs. 1, 2, and 3. We observed that these physical quantities have their maximum values at the centre of the star. They also are positive, continuous, and monotonously decreasing functions of the radial variable r. Moreover, in Fig. 2 we can observe that Eq. (28) is satisfied. Also, the local anisotropy function $\Pi=p_t-p_r$ is positive. This grows as one approaches the radius of the star from the centre (see Fig. 4). Furthermore, we can notice that at the center of the star the anisotropy is zero so there is no collapse and the core of the star tends towards stability. Thus, we have confirmed the physical acceptability of the material sector of our model.

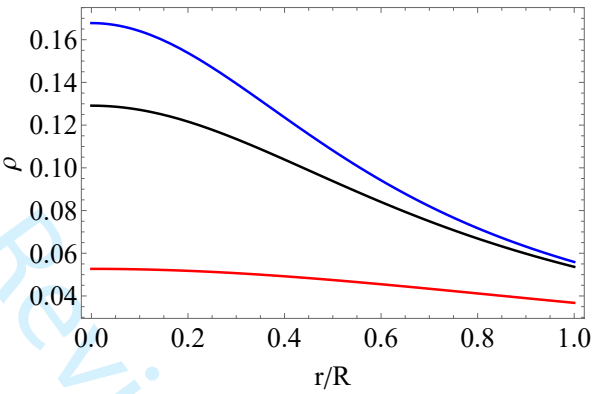

Fig. 1: Energy density profiles

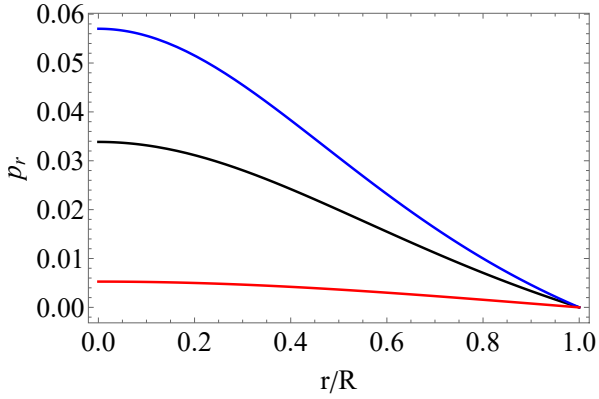

Fig. 2: Radial pressure profiles

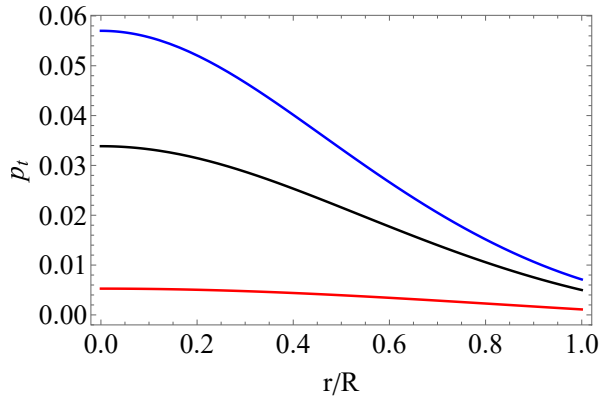

Fig. 3: Tangential pressure profiles

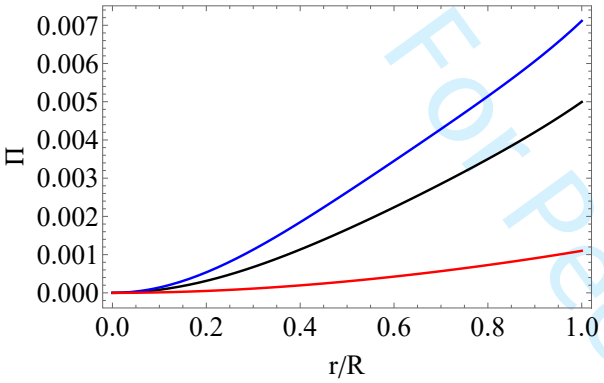

Fig. 4: Anisotropy in pressure profiles

5.1.2 New interior space-time

The spacetime metric components of the interior solution are positive and finite functions. In the centre, the radial metric satisfies $e^{-\lambda(0)} = 1$ and is monotonically decreasing of r (see Fig. 5). While e^{ν} is a monotonously decreasing function of the same variable r and $e^{\nu(0)} =$ constant (see Fig. 6).

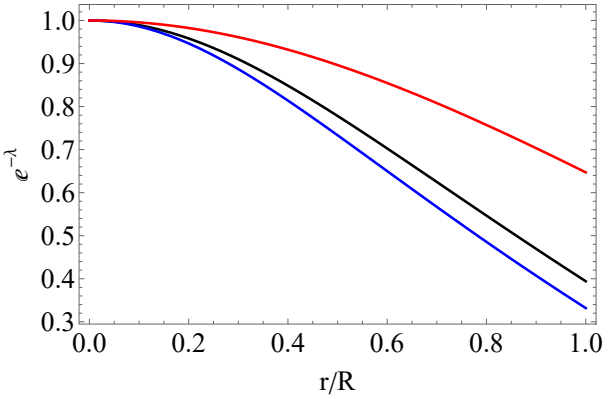

Fig. 5: Radial component of the metric profile

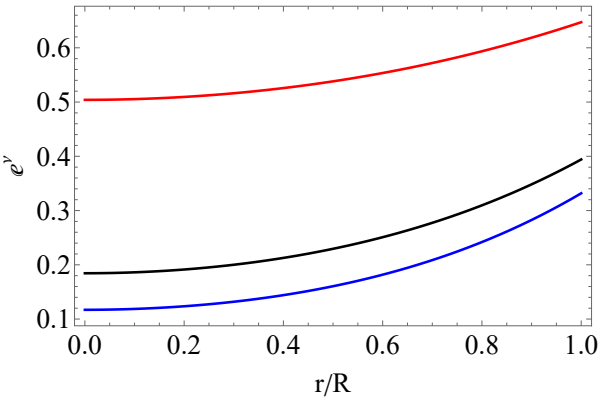

Fig. 6: Temporal component of the metric profile

5.1.3 Energy conditions

In Figs. 7 and 8, we observe that the dominant energy condition given by Eq. (30) is satisfied. Furthermore, in Fig.9, we can observe that the strong energy condition given by Eq. (31) is satisfied for $K = 0.43$ with $u = 0.302917$ (black line) and $K = 0.47$ with $u = 0.176426$ (red line) configurations; this indicates that the model is physically viable. In contrast, for $K = 0.44$ with $u = 0.334079$ (blue line), the SEC is violated, suggesting that this model can be unstable for such a configuration. According to [111], SEC violation can occur in systems with negative pressures or extreme conditions, such as in certain neutron star models.

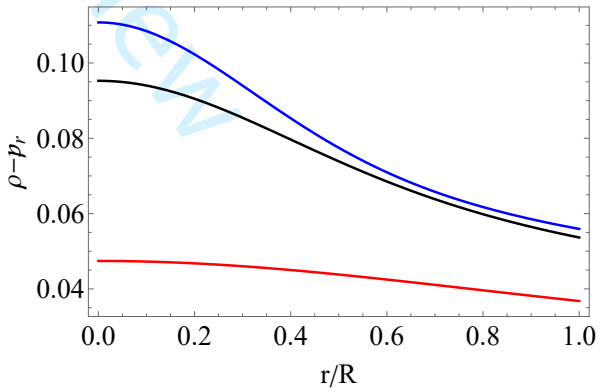

Fig. 7: $\rho - p_r$ profile

5.1.4 Redshift function

In Fig. 10, we notice that Z is positive and is a monotonically decreasing function of the radial variable r. We also see that for the models that comply with the

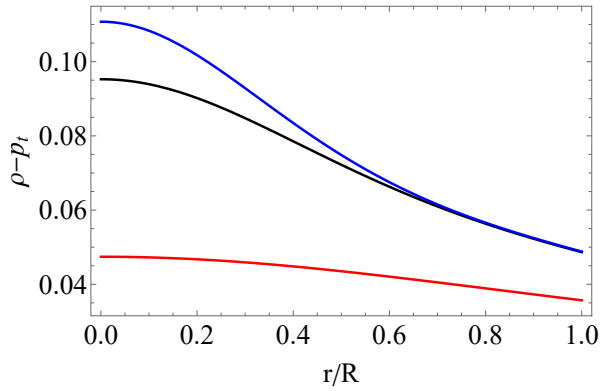

Fig. 8: $\rho - p_t$ profile

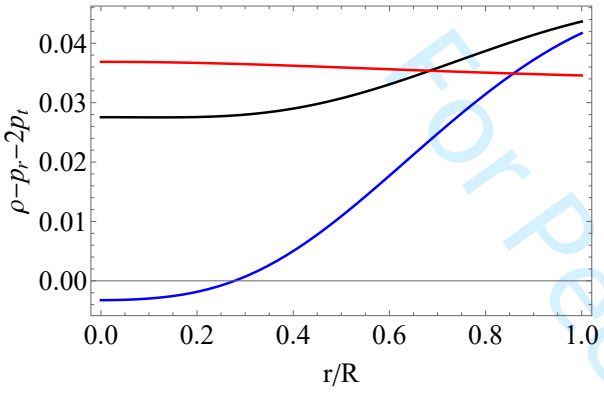

Fig. 9: $\rho - p_r - 2p_t$ profile

SEC (see illustration 9), $K = 0.44$ and $K = 0.47$, and the value on the surface is less than 3.842, fulfilling the acceptability condition 6. While for model $K = 0.43$, since it does not comply with the SEC, it must have a value less than the universal limit of 5.211 on the stellar surface. In fact, this value is $Z = 0.735938$, also fulfilling the mentioned condition.

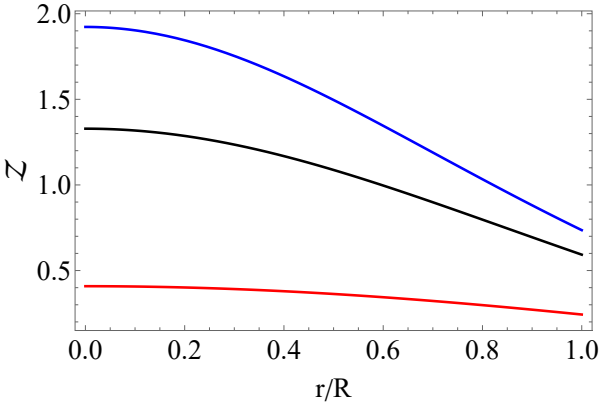

Fig. 10: Redshift function profile

5.1.5 Causality condition

To satisfy this condition, the relationships given by Eq. (29) must be met. We can observe that in Figs. 11 and 12, this condition is indeed fulfilled. This shows that the model meets the causality condition, because the radial velocity v_r^2 and the tangential velocity v_t^2 of sound inside the stellar object do not exceed the causal limit of the speed of light $c = 1$. It is important to note that since these interior sound velocity profiles are not monotonously decreasing functions of the radial variable r, it is possible that the model may have some instability.

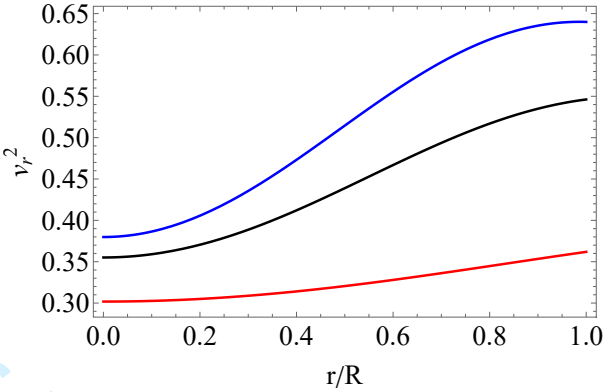

Fig. 11: Radial sound velocity profile

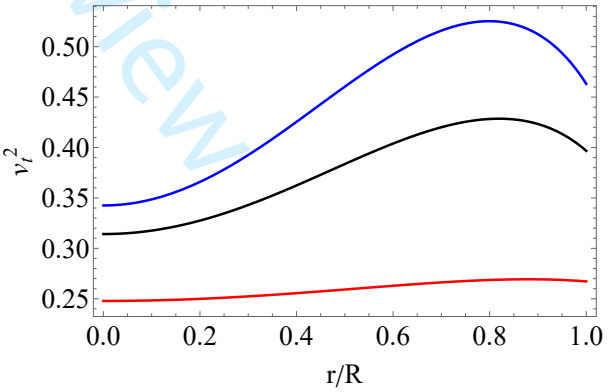

Fig. 12: Tangential sound velocity profile

Before analysing the energy exchange within the stellar compact object modelled by our new interior solution, we see from all this previous analysis that it is physically realistic since it meets all the conditions of physical acceptability for a self-gravitating sphere supported by an anisotropic fluid, at least for the configurations analysed previously.

5.2 Energy exchange between both relativistic fluids

We show the behaviour of ΔE given by Eq. (21) in Fig. 13, namely, the energy interchange between both fluids: the Wyman IIa ($n = 1$) isotropic fluid and the polytrope. It is shown that $\Delta E > 0$, and these interchanges increase for the outer regions of the stellar compact object for the configurations that we considered. Therefore, it can be deduced that the polytrope transfers energy to the environment to achieve coexistence with the perfect fluid within the resulting stellar object. On the other hand, in the stellar centre the energy exchange is null ($\Delta E = 0$), which indicates stability in that region, and this energy exchange increases as the r moves to more external areas of the compact star.

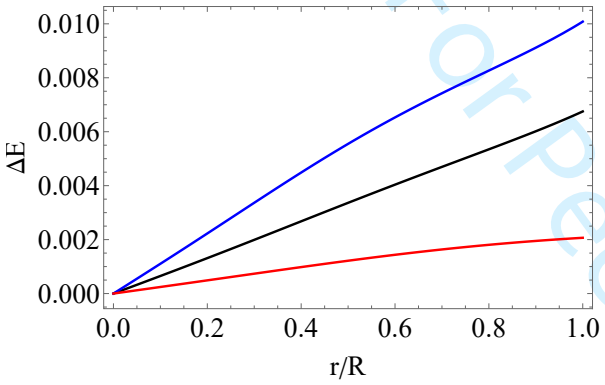

Fig. 13: Energy interchange profile

In Fig. 14, the energy exchange is shown for three values of compactness factors u with fixed $K = 0.43$. This interchange is more elevated for the more compact configurations. Instead, in Fig. 15, the energy exchange is shown for $u = 0.3340$ and three different values of K. We observe that the intensity of the energy exchange is increased as K increases. Therefore, the intensity of the energy exchange between relativistic fluids is favoured with the increase in the value of K and of the compactness factor.

6 Conclusions and remarks

The energetic interaction between two relativistic fluids was analysed, one consisting of an isotropic relativistic polytrope and the other a Wymann IIa-type isotropic fluid, forming a realistic stellar compact object. This was made possible by using the GD via the MGDe framework. Precisely, the seed source considered was a well-known Wymann IIa fluid (with $n = 1$), and the extra source $\Theta_{\mu\nu}$ is a polytrope, and using the algorithm developed in [67] with the use of mimic constraint for energy density, namely, assuming that the energy densities between the interacting fluids are the same, which allowed to found the function g' given by Eq. (41). After that, the numerical integration of g' was carried out, in which values were taken for the different constants involved such as A, B, K, n, so that the stellar model meets all the conditions of physical acceptability for an anisotropic compact star. It is true that one can calculate the material sector of the stellar model only with the value of g' since the EFE depends on ν' and not on ν, but we set out to find real values of g and ν since we also wanted to ensure a physically realistic interior space-time. As a result, three exotic configurations were generated, all consistent with the physical acceptability criteria. However, only two of these configurations fully met the Strong Energy Condition (see Eq. (31)). We checked that for the set of values of $[-1.638; -3.121]$ for g the model is physically viable.

It is importan to mention, that the possibility of using a mimic constraint for the pressure was also viable; however, this did not yield physically realistic results. This does not mean that other types of constraints can be explored to conduct this type of study; the task is not at all easy, but it would be very interesting.

As a main result, we found that for the system to be physically realistic, it is necessary for the polytrope to deliver energy to the environment. Precisely, in the case when a Tolman IV fluid interacts with the polytrope also has the same direction of energy exchange [67], that is, the polytrope releases the energy in order to sostain the self-gravitating sphere compatible with the exterior solution of Schwarzschild. Same thing was also reported in [71], namely, that is necesary the exchange energy is from the polytrope (in such case the isotropic fluid used was the Tolman VII). Thus, we have three coincidencies respect the direction in which a perfect fluid interacts energetically with a relativistic polytrope inside an stellar compact object. It can be thinking the polytrope does a work in order to mantain the fluid polytrope in the interior of the compact star. In a sense, a similar study could be done with another isotropic fluid to be able to answer more precisely whether this direction in which this exchange occurs is the same regardless of the isotropic solution chosen. This task is not at all easy, but it is worth doing since it will answer this question, which we believe, with three coincidences already shown in a hundred ways, already tells us a lot about a certain trend.

Now, the exchange energy in our case is zero in the centre of the stellar object and increases for the outermost regions of the astrophysical object. This behaviour is the same for the Tolman IV case, and it is different

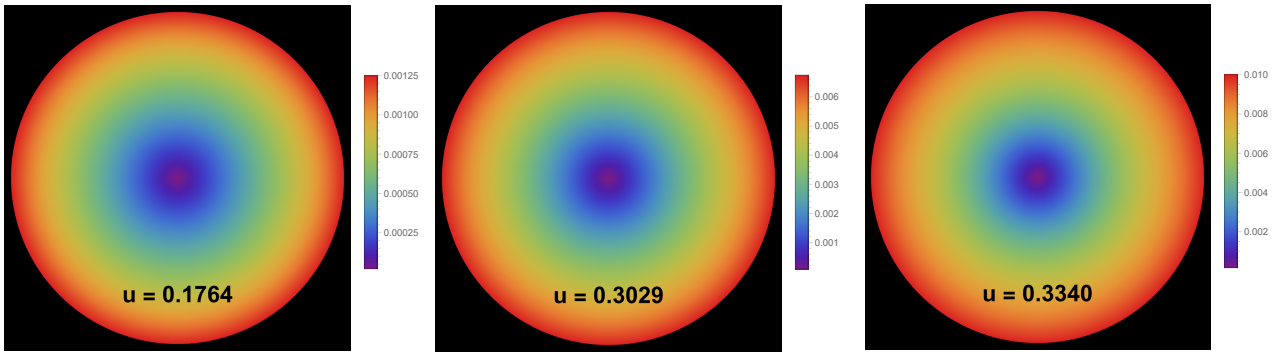

Fig. 14: ΔE density plot for $K = 0.43$ and a) with $u = 0.1764$, b) with $u = 0.3029$, and c) with $u = 0.3340$.

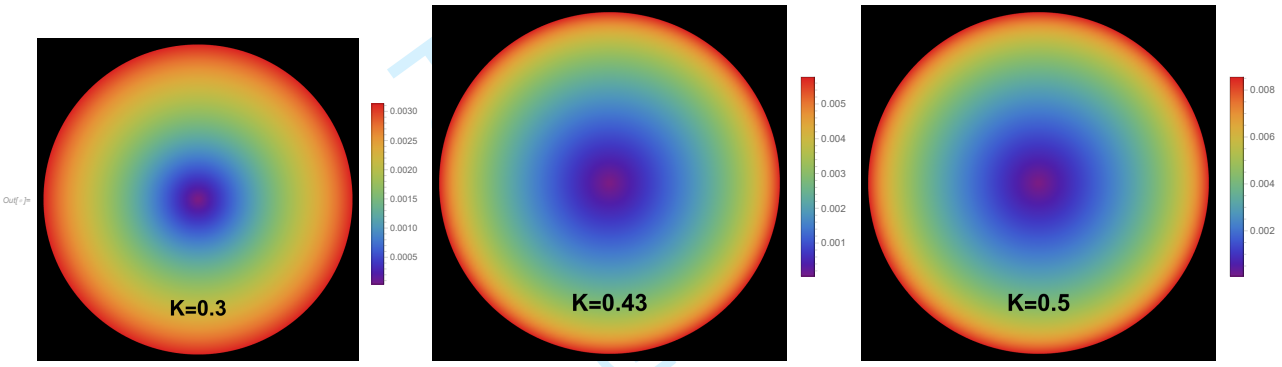

Fig. 15: ΔE density plot for the compactness factor of $u = 0.3340$ with a) $K = 0.30$, b) $K = 0.43$, and c) $K = 0.50$.

in the case of Tolman VII, but the three cases coincides in the fact the energy exchange is null in the centre of the compact star, which suggest it is a mandatory characteristic of these objects. Moreover, we that the energy exchange is more intense for increasingly compact stars and as the values of the constant K increase in our case. It is also important to highlight the possible relationship that anisotropy has with energy exchange; precisely, this is zero in the centre, which may be related to the suppression of energy exchange ($\Delta E = 0$) inside the stellar object. However, in more external areas, the interactions increase, generating anisotropy and consequently an energy exchange. In fact, we have verified that those configurations that do not satisfy the SEC condition have wider external regions than those that do, so that the presence of wider energy exchange zones in some ways accounts for more unstable configurations. This contrast underscores the critical role of the SEC in regulating energy interactions within complex relativistic systems.

We have to emphatize the importance of this work and the mentioned in the above paragraph since the study of the polytropes in general relativity is not an easy task since one have to solve numerically the LaneEmden equations. But with the help of the framework of GD via MGDe such difficulty is avoided in order to study the energy exchange between the fluids that supports a stellar compact object. The way to do it in the case of the isotropic fluid and polytrope was developed by [67] via two mimic constraints is not easy task, also is necessary a numerical approach. We believe that is necessary to carry out investigations about the stability of these compact objects, namely, using diverse criteria of stability. Specifically, can be very worth the study of such objects under radial and non-radial perturbations. It may even be very ambitious to carry out a study on the influence of gravitational cracking on the exchange of both fluids, as has already been done for a specific case in [99]. Clearly, all these types of studies will contribute enormously to our understanding of the physics within stellar remnants, both in their evolution and in their most relevant events.

To further advance the understanding of energy exchange dynamics within compact stellar objects, future research could explore alternative isotropic fluid models interacting with polytropic fluids to determine if

the observed energy transfer trends are universal across different fluid configurations. Investigating the impact of varying polytropic indices and compactness factors on energy exchange could provide deeper insights into the stability and evolution of these systems. Additionally, incorporating non-radial perturbations and gravitational cracking analyses could reveal how structural instabilities influence fluid interactions, potentially uncovering new mechanisms driving stellar evolution. Extending the gravitational decoupling framework to include multi-fluid systems or anisotropic seed solutions may also yield novel stellar models, enhancing our understanding of complex astrophysical phenomena. Finally, leveraging advanced numerical techniques, such as machine learning-driven simulations, could improve the precision of modeling energy exchanges, offering a pathway to explore extreme conditions within stellar remnants.

References

1. A. Einstein, Die Feldgleichungen der Gravitation. Sitzungsber. Knigl. Preuss. Akad. Wiss. Berlin (Math. Phys.), 1915, 844847
2. A. Einstein, Die Feldgleichungen der Gravitation. Sitzungsber. Knigl. Preuss. Akad. Wiss. Berlin (Math. Phys.), 1915, 844847
3. K. Schwarzschild, On the gravitational field of a sphere of incompressible fluid according to Einstein's theory. arXiv:physics/9912033 (1999)
4. K. Schwarzschild, On the gravitational field of a mass point according to Einsteins theory. arXiv:physics/9905030 (1999)
5. R.C. Tolman, Static solutions of einsteins field equations for spheres of fluid. Phys. Rev. **55**(4), 364 (1939)
6. J.R. Oppenheimer, G.M. Volkoff, On massive neutron cores. Phys. Rev. **55**(4), 374 (1939)
7. M. Delgaty, K. Lake, Physical acceptability of isolated, static, spherically symmetric, perfect fluid solutions of Einsteins equations. Comput. Phys. Commun. **115**, 395415 (1998)
8. M.R. Finch, J.E. Skea, A realistic stellar model based on an ansatz of Duorah and Ray. Class. Quantum Grav. **6**, 467 (1989)
9. B. Ivanov, Static charged perfect fluid spheres in general relativity. Phys. Rev. D **65**(10), 104001 (2002)
10. M.H. Murad, N. Pant, A class of exact isotropic solutions of Einsteins equations and relativistic stellar models in general relativity. Astrophys. Space Sci. **350**, 349359 (2014)
11. J. Kumar & P. Bharti, An isotropic compact stellar model in curvature coordinate system consistent with observational data. Eur. Phys. J. Plus, bf 137(3), 330 (2022)
12. M.K. Mak and T. Harko, Isotropic stars in general relativity. Eur. Phys. J. C **73**(10), 2585 (2013)
13. G.G.L. Nashed, Isotropic stellar model in mimetic theory. Gen. Relativ. Gravit. **55**, 63 (2023)
14. J. Andrade & D. Santana, An isotropic extension of Einsteins universe solution through gravitational decoupling. Eur. Phys. J. C, **82**(11), 985 (2022)
15. B.C. Nolan and L.V. Nolan, On isotropic cylindrically symmetric stellar models. Class. and Quantum Grav. **21**(15), 3693 (2004)
16. A. Waseem, S. Naeem, Study of isotropic stellar models via DurgapalLake solutions in Rastall system. Phys. Scr. **99**, 125023 (2024)
17. L. Herrera, N.O. Santos, Local anisotropy in self-gravitating systems. Phys. Rep. **286**, 53130 (1997)
18. R. Kippenhahn, A. Weigert, A. Weiss, Stellar Structure and Evolution, Vol. 192 (Springer-Verlag, Berlin, 1990)
19. A.I. Sokolov, Phase transitions in a superfluid neutron liquid. Sov. Phys. JETP **52**, 575 (1980)
20. R.F. Sawyer, Condensed π^- phase in neutron-star matter. Phys. Rev. Lett. **29**, 382 (1972)
21. H. Heiselberg, M. Hjorth-Jensen, Phases of dense matter in neutron stars. Phys. Rep. **328**, 237327 (2000)
22. J. Binney, S. Tremaine, Galactic Dynamics (Princeton Series in Astrophysics, Princeton, 1987)
23. P.S. Letelier, Anisotropic fluids with two-perfect-fluid components. Phys. Rev. D **22**, 807 (1980)
24. R.P. Pant, S. Gedela, R.K. Bisht, N. Pant, Core-envelope model of super dense star with distinct equation of states. Eur. Phys. J. C **79**, 602 (2019)
25. N. Pant, S. Gedela, R.P. Pant, J. Upreti, R.K. Bisht, Three-layered relativistic stellar model endowed with distinct equation of states. Eur. Phys. J. Plus **135**, 180 (2020)
26. S.S. Yazadjiev, Relativistic models of magnetars: Nonperturbative analytical approach. Phys. Rev. D **85**, 044030 (2012)
27. R. Ciolfi, V. Ferrari, L. Gualtieri, Structure and deformations of strongly magnetized neutron stars with twisted-torus configurations. Mon. Not. R. Astron. Soc. **406**, 25402548 (2010)
28. J. Frieben, L. Rezzolla, Equilibrium models of relativistic stars with a toroidal magnetic field. Mon. Not. R. Astron. Soc. **427**, 34063426 (2012)
29. V. Canuto, Equation of state at ultrahigh densities. Annu. Rev. Astron. Astrophys. **12**, 167214 (1974)
30. L. Herrera, A. Di Prisco, J. Hernndez-Pastora, N.O. Santos, On the role of density inhomogeneity and local anisotropy in the fate of spherical collapse. Phys. Lett. A **237**, 113118 (1998)
31. L. Herrera, Stability of the isotropic pressure condition. Phys. Rev. D **101**(10), 104024 (2020)
32. J.H. Jeans, The motions of stars in a Kapteyn universe. Mon. Not. R. Astron. Soc. **82**, 122132 (1922)
33. G. Lematre, Ann. Soc. Sci. Brux. A **53**, 51 (1933)
34. R.L. Bowers, E.P.T. Liang, Anisotropic spheres in general relativity. Astrophys. J. **188**, 657 (1974)
35. K. Dev & M. Gleiser, Anisotropic stars: exact solutions. Gen. Relativ. Gravit., **34**(11), 17931818(2002)
36. M.K. Mak, T. Harko, An exact anisotropic quark star model. Chin. J. Astron. Astrophys. **2**, 248 (2002)
37. S.K. Maurya & S.D. Maharaj, Anisotropic fluid spheres of embedding class one using Karmarkar condition. Eur. Phys. J. C, **77**(5), 328(2017)
38. M. Malaver, Some new models of anisotropic compact stars with quadratic equation of state. World Sci. News **109**, 180194 (2018)
39. R.N. Nasheeha, S. Thirukkanesh, F.C. Ragel, Anisotropic models for compact star with various equation of state. Eur. Phys. J. Plus **136**, 132 (2021)
40. M. Kumar, J. Kumar, P. Bharti, A.K. Prasad, Exploring the physics of relativistic compact stars: an anisotropic model with quadratic equation of state in Buchdahl geometry. Astrophys. Space Sci. **369**, 97 (2024)

41. K. Pant, P. Fuloria, A comprehensive analysis of anisotropic stellar objects with quadratic equation of state. Pramana **98**, 158 (2024)
42. S. Das, K.N. Singh, L. Baskey, F. Rahaman, A.K. Aria, Modeling of compact stars: an anisotropic approach. Gen. Relativ. Gravit. **53**, 25 (2021)
43. J. Zdunik, P. Haensel, Maximum mass of neutron stars and strange neutron-star cores. Astron. Astrophys. **551**, A61 (2013)
44. J. M. Lattimer & M. Prakash, The physics of neutron stars. Science, **304**(5670), 536-542(2004)
45. J.M. Lattimer, M. Prakash, The equation of state of hot, dense matter and neutron stars. Phys. Rep. **621**, 127164 (2016)
46. F. zel, P. Freire, Masses, radii, and the equation of state of neutron stars. Annu. Rev. Astron. Astrophys. **54**, 401440 (2016)
47. G. Baym, T. Hatsuda, T. Kojo, P.D. Powell, Y. Song, T. Takatsuka, From hadrons to quarks in neutron stars: a review. Rep. Prog. Phys. **81**, 056902 (2018)
48. C.J. Horowitz, M.A. Perez-Garcia, J. Piekarewicz, Neutrino-pasta scattering: The opacity of nonuniform neutron-rich matter. Phys. Rev. C **69**, 045804 (2004)
49. M. Caplan, C. Horowitz, Colloquium: Astromaterial science and nuclear pasta. Rev. Mod. Phys. **89**, 041002 (2017)
50. C. Kouvaris, P. Tinyakov, Can neutron stars constrain dark matter?. Phys. Rev. D **82**, 063531 (2010)
51. J. Bramante, T. Linden, Detecting dark matter with imploding pulsars in the galactic center. Phys. Rev. Lett. **113**(19), 191301 (2014)
52. H. Sotani, K. Kokkotas, N. Stergioulas, Torsional oscillations of relativistic stars with dipole magnetic fields. Mon. Not. R. Astron. Soc. **375**, 261277 (2007)
53. T. Kuroda, M. Shibata, Failed supernova simulations beyond black hole formation. Mon. Not. R. Astron. Soc. **526**, 152159 (2023)
54. D. Tsuna, Failed supernova remnants. Publ. Astron. Soc. Jpn. **73**, L6L11 (2021)
55. C.S. Kochanek, Failed supernovae explain the compact remnant mass function. Astrophys. J. **785**, 28 (2014)
56. C.L. Fryer, P.J. Brown, F. Bufano, J.A. Dahl, C.J. Fontes, L.H. Frey, , P.A. Young, Spectra and light curves of failed supernovae. Astrophys. J. **707**, 193 (2009)
57. J. Neustadt, C. Kochanek, K. Stanek, C. Basinger, T. Jayasinghe, C. Garling, S. Adams, J. Gerke, The search for failed supernovae with the Large Binocular Telescope: a new candidate and the failed SN fraction with 11 yr of data. Mon. Not. R. Astron. Soc. **508**, 516528 (2021)
58. E. OConnor, C.D. Ott, Black hole formation in failing core-collapse supernovae. Astrophys. J. **730**, 70 (2011)
59. R. Fernndez, E. Quataert, K. Kashiyama, E.R. Coughlin, Mass ejection in failed supernovae: variation with stellar progenitor. Mon. Not. R. Astron. Soc. **476**, 23662383 (2018)
60. S.C. Rose, S. Naoz, R.E. Sari, I. Linial, The formation of intermediate-mass black holes in galactic nuclei. Astrophys. J. Lett. **929**, L22 (2022)
61. F.P. Rizzuto, et al., Intermediate mass black hole formation in compact young massive star clusters. Mon. Not. R. Astron. Soc. **501**, 52575273 (2021)
62. Y. Sakurai, N. Yoshida, M.S. Fujii, S. Hirano, Formation of intermediate-mass black holes through runaway collisions in the first star clusters. Mon. Not. R. Astron. Soc. **472**, 16771684 (2017)
63. M.S. Fujii, L. Wang, A. Tanikawa, Y. Hirai, T.R. Saitoh, Simulations predict intermediate-mass black hole formation in globular clusters. Science **384**, 14881492 (2024)
64. J.E. Greene, J. Strader, L.C. Ho, Intermediate-mass black holes. Annu. Rev. Astron. Astrophys. **58**, 257312 (2020)
65. K. Ruiz-Rocha, et al., Properties of Lite Intermediate-mass Black Hole Candidates in LIGO-Virgos Third Observing Run. Astrophys. J. Lett. **985**, L37 (2025)
66. K. Ruiz-Rocha, K. Holley-Bockelmann, K. Jani, M. Mapelli, S. Dunham, W. Gabella, A Sea of Black Holes: Characterizing the LISA Signature for Stellar-origin Black Hole Binaries. Astrophys. J. **981**, 27 (2025)
67. J. Ovalle, E. Contreras, Z. Stuchlk, Energy exchange between relativistic fluids: the polytropic case. Eur. Phys. J. C **82**, 211 (2022)
68. J. Ovalle, Searching exact solutions for compact stars in braneworld: a conjecture. Mod. Phys. Lett. A **23**, 32473263 (2008)
69. J. Ovalle, Decoupling gravitational sources in general relativity: The extended case. Phys. Lett. B, **788**, 213-218(2019)
70. J. Ovalle, Decoupling gravitational sources in general relativity: from perfect to anisotropic fluids. Phys. Rev. D **95**, 104019 (2017)
71. E. Contreras, Z. Stuchlk, Energy exchange between Tolman VII and a polytropic fluid. Eur. Phys. J. C **82**, 365 (2022)
72. S.K. Maurya, M. Govender, G. Mustafa, R. Nag, Relativistic models for vanishing complexity factor and isotropic star in embedding Class I spacetime using extended geometric deformation approach. Eur. Phys. J. C **82**, 1006 (2022)
73. T.T. Smitha, S.K. Maurya, B. Dayanandan, G. Mustafa, Anisotropic star by gravitational decoupling: a vanishing complexity approach. Results Phys. **49**, 106502 (2023)
74. M.A. Habsi, S.K. Maurya, S.A. Badri, M. Al-Alawiya, T.A. Mukhaini, H.A. Malki, G. Mustafa, Self-bound embedding Class I anisotropic stars by gravitational decoupling within vanishing complexity factor formalism. Eur. Phys. J. C **83**, 286 (2023)
75. S.K. Maurya, A. Errehymy, M.K. Jasim, M. Daoud, N. Al-Harbi, A.H. Abdel-Aty, Complexity-free solution generated by gravitational decoupling for anisotropic self-gravitating star in symmetric teleparallel f(Q)-gravity theory. Eur. Phys. J. C **83**, 317 (2023)
76. S.V. Lohakare, S.K. Maurya, K.N. Singh, B. Mishra, A. Errehymy, Influence of three parameters on maximum mass and stability of strange star under linear f(Q)- action. Mon. Not. R. Astron. Soc. **526**, 37963814 (2023)
77. S.K. Maurya, K.N. Singh, M. Govender, S. Ray, ComplexityFree Anisotropic Solution of Buchdahl's Model and Energy Exchange Between Relativistic Fluids by Extended Gravitational Decoupling. Fortschr. Phys. **71**, 2300023 (2023)
78. E. Contreras & Z. Stuchlik, A simple protocol to construct solutions with vanishing complexity by Gravitational Decoupling. Eur. Phys. J. C, **82**(8), 706(2022)
79. J. Andrade, D. Santana, Energetic interaction between Einsteins universe and a source like-Tolman IV complexity factor. Int. J. Theor. Phys. **63**, 134 (2024)
80. J. Ovalle, R. Casadio, Beyond Einstein gravity: the minimal geometric deformation approach in the brane-world. Springer Nature, Cham (2020)
81. R. da Rocha, Dark SU(N) glueball stars on fluid branes. Phys. Rev. D **95**, 124017 (2017)
82. A. FernandesSilva & R.D. Rocha, GregoryLaflamme analysis of MGD black strings. Eur. Phys. J. C, **78**(3), 271(2018)

83. R. Casadio, P. Nicolini, R. da Rocha, Generalised uncertainty principle Hawking fermions from minimally geometric deformed black holes. Class. Quantum Grav. **35**, 185001 (2018)
84. A. Fernandes-Silva, A.J. Ferreira-Martins, R. da Rocha, The extended minimal geometric deformation of SU(N) dark glueball condensates. Eur. Phys. J. C **78**, 631 (2018)
85. E. Contreras, P. Bargueo, Minimal geometric deformation decoupling in 2+1 dimensional spacetimes. Eur. Phys. J. C **78**, 558 (2018)
86. E. Contreras, Minimal Geometric Deformation: the inverse problem. Eur. Phys. J. C, **78**(8), 678(2018)
87. E. Contreras & P. Bargueo, Minimal geometric deformation in asymptotically (A-) dS space-times and the isotropic sector for a polytropic black hole. Eur. Phys. J. C, **78**(12), 985(2018)
88. R. Da Rocha & A.A. Tomaz, Holographic entanglement entropy under the minimal geometric deformation and extensions. Eur. Phys. J. C, **79**(12), 1035(2019)
89. C. Las Heras, P. Len, New algorithms to obtain analytical solutions of Einsteins equations in isotropic coordinates. Eur. Phys. J. C **79**, 990 (2019)
90. G. Panotopoulos, . Rincn, Minimal geometric deformation in a cloud of strings. Eur. Phys. J. C **78**, 851 (2018)
91. . Rincn, L. Gabbanelli, E. Contreras, F. Tello-Ortiz, Minimal geometric deformation in a ReissnerNordstrm background. Eur. Phys. J. C **79**, 873 (2019)
92. R. da Rocha, MGD Dirac stars. Symmetry **12**, 508 (2020)
93. E. Contreras, F. Tello-Ortiz, S.K. Maurya, Regular decoupling sector and exterior solutions in the context of MGD. Class. Quantum Grav. **37**, 155002 (2020)
94. C. Arias, F. Tello-Ortiz, E. Contreras, Extra packing of mass of anisotropic interiors induced by MGD. Eur. Phys. J. C **80**, 463 (2020)
95. R. da Rocha, Minimal geometric deformation of Yang-Mills-Dirac stellar configurations. Phys. Rev. D, **102**(2), 024011(2020)
96. R. da Rocha & A.A. Tomaz, MGD-decoupled black holes, anisotropic fluids and holographic entanglement entropy. Eur. Phys. J. C, **80**(9), 857(2020)
97. P. Meert, R. da Rocha, Probing the minimal geometric deformation with trace and Weyl anomalies. Nucl. Phys. B **967**, 115420 (2021)
98. S.K. Maurya, K.N. Singh, M. Govender, S. Hansraj, Gravitationally decoupled strange star model beyond the standard maximum mass limit in EinsteinGaussBonnet gravity. Astrophys. J. **925**, 208 (2022)
99. S.S. Medina, J. Andrade, D. Santana, T. Naseer, Effect of gravitational cracking on energy exchange in relativistic fluids: a first approach. Eur. Phys. J. C **85**, 113 (2025)
100. M. Wyman, Schwarzschild interior solution in an isotropic coordinate system. Phys. Rev. **70**, 74 (1946)
101. J. Andrade & E. Contreras, Stellar models with like-Tolman IV complexity factor. Eur. Phys. J. C, **81**(10), 889(2021)
102. J. Andrade, D. Andrade, Stellar models with like-Wyman IIa complexity factor. J. Phys.: Conf. Ser. **2796**, 012007 (2024)
103. D. Santana, E. Fuenmayor, E. Contreras, Integration of the LaneEmden equation for relativistic anisotropic polytropes through gravitational decoupling: a novel approach. Eur. Phys. J. C **82**, 703 (2022)
104. G. Abelln, E. Fuenmayor, L. Herrera, The double polytrope for anisotropic matter: Newtonian case. Phys. Dark Univ. **28**, 100549 (2020)
105. L. Herrera & W. Barreto, Newtonian polytropes for anisotropic matter: General framework and applications. Phys. Rev. D, **87**(8), 087303(2013)
106. G.P. Horedt, Polytropes: applications in astrophysics and related fields. Springer, Dordrecht (2004)
107. B.V. Ivanov, Analytical study of anisotropic compact star models. Eur. Phys. J. C, **77**(11), 738(2017)
108. B.V. Ivanov, Maximum bounds on the surface redshift of anisotropic stars. Phys. Rev. D **65**, 104011 (2002)
109. H.A. Buchdahl, General relativistic fluid spheres. Phys. Rev. **116**, 1027 (1959)
110. W. Gander, W. Gautschi, Adaptive quadrature-revisited. BIT Numer. Math. **40**, 84101 (2000)
111. M. Visser, C. Barcelo, Energy conditions and their cosmological implications. In: 3rd Int. Conf. on Particle Phys. and the Early Universe, pp. 98112 (2000, September)